CONFIDENTIAL

Copy
RM H55E26

NACA RM H55E26

AUTHOR'S PERSONAL COPY

NACA

RESEARCH MEMORANDUM

FLIGHT MEASUREMENTS OF THE LATERAL RESPONSE CHARACTERISTICS OF THE CONVAIR XF-92A DELTA-WING AIRPLANE

By Euclid C. Holleman

High-Speed Flight Station
Edwards, Calif.

CLASSIFICATION CHANGED TO UNCLASSIFIED
AUTHORITY: NACA RESEARCH ABSTRACT NO. 127
EFFECTIVE DATE: MAY 16, 1958
WHL

CLASSIFIED DOCUMENT

This material contains information affecting the National Defense of the United States within the meaning of the espionage laws, Title 18, U.S.C., Secs. 793 and 794, the transmission or revelation of which in any manner to an unauthorized person is prohibited by law.

NATIONAL ADVISORY COMMITTEE FOR AERONAUTICS

WASHINGTON

August 5, 1955

CONFIDENTIAL

NATIONAL ADVISORY COMMITTEE FOR AERONATUICS

RESEARCH MEMORANDUM

FLIGHT MEASUREMENTS OF THE LATERAL RESPONSE CHARACTERISTICS OF THE CONVAIR XF-92A DELTA-WING AIRPLANE

By Euclid C. Holleman

SUMMARY

As part of the flight research program conducted with the Convair XF-92A delta-wing research airplane, rudder pulse maneuvers were obtained at an altitude of about 30,000 feet over a Mach number range of 0.52 to 0.92. Tests were made with and without a wing fence.

By analyzing these maneuvers the characteristics of the airplane transient, airplane stability derivatives, and frequency-response characteristics were measured. The airplane handling qualities were improved by the addition of wing fences. The agreement between experimental and calculated stability derivatives was fair to poor. However by using transfer-function equations from the lateral equations of motion and the experimental stability derivatives, frequency responses were calculated that compared favorably with those determined by Fourier transformation.

INTRODUCTION

Measurements of the dynamic lateral response characteristics of the airplane were made at an altitude of about 30,000 feet and over a Mach number range of 0.52 to 0.92 as part of a flight investigation using the XF-92A delta-wing airplane. Some dynamic lateral response data were also obtained while the effects of wing fences on the airplane longitudinal characteristics were being investigated. Results of the longitudinal stability investigation with and without wing fences are presented in reference 1. The results of simultaneous lateral tests on the airplane are reported in reference 2, and results of dynamic longitudinal tests are presented in reference 3.

During this phase of the XF-92A test program the dynamic lateral behavior of the airplane was investigated by analyzing the airplane

response to abrupt rudder pulse disturbances. From the recording of each of these maneuvers it was possible to obtain some of the more important stability derivatives and also the frequency-response characteristics of the airplane.

SYMBOLS AND COEFFICIENTS

a_t transverse acceleration, g units

b wing span, ft

h_p pressure altitude, ft

C_l rolling-moment coefficient

C_n yawing-moment coefficient

C_Y side-force coefficient

$$C_{l_\beta} = \frac{\partial C_l}{\partial \beta}$$

$$C_{l_p} = \frac{\partial C_l}{\partial \frac{pb}{2V}}$$

$$C_{l_r} = \frac{\partial C_l}{\partial \frac{rb}{2V}}$$

$$C_{l_{\delta_r}} = \frac{\partial C_l}{\partial \delta_r}$$

$$C_{n_p} = \frac{\partial C_n}{\partial \frac{pb}{2V}}$$

$$C_{n_r} = \frac{\partial C_n}{\partial \frac{rb}{2V}}$$

$C_{n_\beta} = \frac{\partial C_n}{\partial \beta}$

$C_{n_{\delta_r}} = \frac{\partial C_n}{\partial \delta_r}$

$C_{Y_\beta} = \frac{\partial C_Y}{\partial \beta}$

$C_{Y_{\delta_r}} = \frac{\partial C_Y}{\partial \delta_r}$

I_X moment of inertia about longitudinal stability axis, slug-ft^2

I_Z moment of inertia about vertical stability axis, slug-ft^2

I_{XZ} product of inertia relative to the stability axis, slug-ft^2

M Mach number

t time, sec

V true velocity, ft/sec

α angle of attack, deg

β sideslip angle, radians or deg

δ_r rudder control position, deg

ϵ angle between reference axis and principal axis, positive when reference axis is above principal axis at nose of airplane, deg

ζ damping ratio

φ roll angle, radians

$\dot{\varphi}$ roll velocity, radians/sec

Φ phase angle, deg

ψ yaw angle, radians

$\dot{\psi}$ yaw velocity, radians/sec

ω frequency, radians/sec

ω_n undamped natural frequency, radians/sec

Subscripts:

b body axis

AIRPLANE

The Convair XF-92A airplane is a single-place fighter-type delta-wing airplane powered by a J33-A-29 turbojet engine with afterburner. Physical characteristics of the airplane are presented in table I and a three-view sketch is presented in figure 1. For some of the tests a fence was located at the 0.607 semispan station of the wing. The fence height was equal to the wing thickness at the 0.607 semispan station and extended around the wing leading edge as shown in figure 2. The airplane inertia in roll and yaw about the body axis was obtained from the manufacturer. An inclination of the principal axis of inertia was estimated to be 1° below the airplane body axis (fig. 1) and the airplane inertia about the stability axis was calculated for the angle-of-attack range of these tests (fig. 3). Airplane weight and center-of-gravity position were determined from pilot reports of the amount of fuel remaining at the conclusion of each maneuver. Average values for these quantities are 13,400 pounds and 27.5 percent of the mean aerodynamic chord, respectively.

The airplane is controlled by a conventional rudder and by full-span elevons which function as elevators and ailerons. All control surfaces are operated by an irreversible hydraulic system with artificial feel.

INSTRUMENTATION

Standard NACA recording instrumentation was used to record airspeed, altitude, normal acceleration, transverse acceleration, yawing velocity, rolling velocity, angle of attack, angle of sideslip, elevon position, and rudder position. All records were synchronized by a common timer at

intervals of 0.1 second. An airspeed head, mounted on a boom approximately 5.4 feet ahead of the airplane nose inlet, measured both static and total pressure. Airspeed was calibrated by pacer and radar tracking and is believed to be accurate to ±0.01 Mach number. Control positions were measured by standard control position transmitters and were recorded on a Weston galvanometer which had a flat response to about 5 cycles per second. Angle of attack and angle of sideslip were measured by a vane-type pickup and were also recorded on a Weston galvanometer. The sideslip vane pickup and recorder had a flat response to about 5 cycles per second. Roll angular velocity was recorded with a direct recording magnetically damped turnmeter with a natural frequency of 20 cycles per second and a damping ratio of 0.64. Yaw angular velocity was recorded with the same type instrument with a natural frequency of 9.5 cycles per second and a damping ratio of 0.67.

TESTS

The test procedure for this investigation consisted of recording the airplane response to abrupt rudder pulses. In each instance the airplane was stabilized at the desired test speed and altitude and was disturbed by a rapid pulse of the rudder control. During the disturbance all controls except the rudder were fixed and following the disturbance all controls were fixed until the airplane returned to stabilized flight. Figure 4 shows typical histories of the test maneuver. Tests, with and without a wing fence, were conducted at 30,000 feet over a Mach number range of 0.52 to 0.92.

METHODS OF ANALYSIS

With the present trends in designing high-performance airplanes it has become apparent that motions other than yaw or sideslip are important in determining acceptable dynamic flying qualities. Reference 4 indicated that roll-to-sideslip ratio might be important in pilot rating of the flying qualities of airplanes. In reference 5 the roll-to-yaw ratio was shown to be useful in determining airplane stability derivatives. Consequently measurements of the amplitudes of roll, yaw, and sideslip have been made from the recorded transients, and have been utilized in the analysis to give airplane stability derivatives. Amplitude ratios and phase relationships of the transient rolling velocity, yawing velocity, and sideslip angle response to rudder pulses have been measured from recorded time histories. However, inasmuch as the recorded time histories are relative to the airplane body axis, they were converted to stability axis data before proceeding with the analysis. This was done by employing the relation $\dot{\psi} = \dot{\psi}_b \cos \alpha - \dot{\phi}_b \sin \alpha$. For the

angle-of-attack range of these tests it was necessary to convert only the yaw velocity to the new axis, since the correction to sideslip and roll velocity was of the order of 1 percent or less. The order of the correction to the yaw velocity is shown in figure 4.

The procedure for determining the amplitude ratios at the airplane natural frequency is graphical in that the free oscillation record is enclosed by an envelope to establish the exponential order of the motion. For each maneuver a plot such as figure 5 is obtained from which the amplitude ratios $\left|\frac{\dot{\phi}}{\dot{\psi}}\right|$, $\left|\frac{\dot{\phi}}{\beta}\right|$, and $\left|\frac{\dot{\psi}}{\beta}\right|$ and the time to damp to one-half amplitude are measured. By careful insepction of the time history, the phase relationships and frequency of the oscillation are determined. The measured amplitude ratios and phase angles were converted to displacement ratios by the usual relationships involving undamped natural frequency and damping angle $\left|\frac{\phi}{\beta}\right| = \frac{1}{\omega_n}\left|\frac{\dot{\phi}}{\beta}\right|$ and $\varphi_{\left|\frac{\phi}{\beta}\right|} = \varphi_{\left|\frac{\dot{\phi}}{\beta}\right|} - (90^\circ + \text{damping angle})$.

It was shown in reference 5 that the stability derivatives, C_{l_β}, C_{l_p}, C_{n_r}, C_{n_β} could be derived from the airplane lateral transient motions. The computing procedure involves the use of an initial approximation for C_{l_β} and C_{l_p}, the measured natural frequency, damping ratio, and estimates for the derivatives of lesser importance $\left(C_{n_p}, C_{Y_\beta}, C_{l_r}\right)$ to calculate the roll-to-yaw amplitude ratio and phase angle. The solution is one of iteration in that C_{l_β} and C_{l_p} are altered until the calculated amplitude ratio and phase angle match those measured experimentally. When the experimental amplitude ratio and phase angle are matched, the values of C_{n_β} and C_{n_r}, as well as C_{l_β} and C_{l_p}, have been determined.

Reference 6 presents a procedure whereby the airplane stability derivatives may be determined from the airplane frequency-response data by utilizing a method of least squares. Sample calculations were made using this method as a check of the results of the previous method.

By means of the Fourier integral $F(\omega) = \int_0^\infty f(t)e^{-i\omega t}dt$ the functions of time were transformed into frequency functions. For this analysis the integral was evaluated by an IBM calculating machine utilizing the method of reference 7. Briefly, the method of integration fits a parabola through the data ordinates and evaluates the integral by

multiplying the ordinates by a set of coefficients. Summing these products evaluates the integral. From these calculations the amplitude and phase angle of the complex components were determined and are presented as ratios of output to input and the difference in output to input phase angle.

RESULTS AND DISCUSSION

By using the methods briefly described in the preceding section, the transient-response data have been analyzed to give airplane stability derivatives and frequency-response characteristics. The transient-response characteristics of the airplane at an altitude of 30,000 feet over a Mach number range of 0.52 to 0.92 are presented in figures 6 to 8. Figure 6 shows the variation with Mach number of roll-to-yaw, roll-to-sideslip, and yaw-to-sideslip amplitude ratio at the natural frequency. The addition of the wing fence reduced the roll-to-yaw and roll-to-sideslip ratios slightly at a Mach number of 0.85. The pilot considered this reduction to be an improvement in the airplane handling qualities at this test condition. Phase angle relationships were also measured and are shown in figure 7. Only the amplitude and phase angle of roll to yaw were used in the present analysis (by the method of ref. 5); however, the amplitudes and phase angles of roll to sideslip and yaw to sideslip are also presented in figures 6 and 7 to show the trends. Figure 8 shows the airplane undamped natural frequency and damping ratio for these test conditions. The measurement of these quantities by the graphical method employed here depends entirely on the airplane response being lightly damped.

By the method of reference 5 the more significant stability derivatives C_{l_β}, C_{n_β}, C_{n_r}, and C_{l_p} were determined and are presented in figure 9. The value of C_{Y_β} was determined by taking the slope of the transverse acceleration plotted against sideslip during the airplane's free oscillation. The variations of these derivatives with Mach number are compared with derivatives calculated by determining the lift-curve slope of the vertical tail (refs. 8 and 9) and by calculating its contribution to the lateral derivatives by the method of reference 10. In these calculations, the vertical tail area was taken as the area above the fuselage. Wing contributions to the derivatives were estimated from the methods of references 8, 11, and 12. The wing and tail contributions to the derivatives were summed without regard for interference effects. The measured sideslip derivatives are compared to those calculated in figure 9(a). Experimental values of C_{Y_β} are approximately 25 percent higher than calculated. Thus it appears that the fuselage or perhaps

interference effects contribute a considerable amount to this derivative. Experimental C_{n_β} shows a different trend than predicted, increasing slightly with Mach number whereas the calculated derivative decreases with Mach number for this test range. Trends in C_{l_β} are similar but the experimental derivative is approximately one-half the calculated derivative. It appears, then, that the simple theory used herein is inadequate in calculating these derivatives. Indicated differences may be the result of influence of the wing wake on the vertical tail since these effects were not considered in the calculations. The experimental C_{n_r} (fig. 9(b)) is many times larger than the calculated damping in yaw. A similar discrepancy was noted in reference 13, particularly at high angles of attack, and was attributed to the wing vortex flow creating sidewash over the rear portion of the fuselage. The sidewash lags the airplane oscillation and increases the tail damping by increasing the angle of attack of the tail during the oscillation. The experimental damping in roll C_{l_p} (fig. 9(c)) compares favorably with the calculated value.

Since the experimental derivatives are functions of the estimated derivatives as well as the measured oscillation characteristics of the airplane, calculations were made to indicate the effect of a nominal change in the calculated derivatives on the experimental derivatives. Results of these calculations are given in table II. The maximum effect of changing C_{n_p} by 20 percent appears in C_{n_r} but this change is only of the order of 5 percent. Altering C_{l_r} changed each of the derivatives but the change was negligible. Twenty-percent change in C_{Y_β} also altered each of the derivatives, the maximum change of the order of 5 percent occurring in C_{l_p}. Thus it appears that fairly accurate experimental derivatives can be obtained with reasonable estimates for the other derivatives. The estimate of the airplane inertia characteristics is also important. For example, the product of inertia estimate will influence C_{n_r} and C_{n_β}. Of course accurate measurements of the motion amplitude ratios and phase angles are necessary. In an attempt to minimize these errors, faired values for these quantities for each Mach number were used in the calculation procedure.

Some results of calculating derivatives by the method of reference 6 are also included in figure 9. The agreement between the derivatives calculated by the methods of references 5 and 6 is considered good at the low Mach number but differences are apparent at the higher Mach number, particularly in C_{n_r} and C_{l_p}. A measure of the control effectiveness was also obtained from the method of reference 6 and is compared to that measured in the Ames 40- by 80-foot wind tunnel in figure 10.

By using the Fourier transformation the frequency content of the transient records has been computed. An example is shown in figure 11. Assuming that the most significant source of error is the reduction of the film record to digital form, error boundaries have been computed as in reference 14 and are also shown in figure 11. It is evident that at the higher frequencies as the frequency content becomes low, (the expected percentage error becomes high) the phase angles tend to diverge. Thus accuracy in amplitude assures accuracy in phase angle. This criterion has been used in terminating the fairings of the transfer functions presented.

Shown in figure 12 is a summary of the frequency-response characteristics of the airplane for four Mach numbers 0.52, 0.63, 0.72, and 0.87 at an altitude of about 30,000 feet. These data show that the natural frequency and peak amplitude ratio of the airplane increase with increasing Mach number for this Mach number range.

The results of the transient analysis and frequency-response analysis were compared by calculating the frequency-response characteristics of the airplane for the test conditions of figure 12. Transfer-function equations derived from the three lateral equations of motion were used with the experimental stability derivatives and the calculated derivatives where experimental derivatives were not available. The inertia characteristics used were from figure 3. The control effectiveness parameters were obtained from tests of the airplane in the Ames 40- by 80-foot wind tunnel (fig. 10). Results of these calculations at one test Mach number (0.63) are shown in figure 13. The agreement shown is considered fairly good. Similar agreement was obtained at the other test Mach numbers.

CONCLUDING REMARKS

By analyzing rudder pulse maneuvers with the XF-92A airplane, the characteristics of the airplane transient, airplane stability derivatives, and transfer functions were measured. An improvement in the airplane handling was noted as a result of the addition of the wing fences. Stability derivatives were evaluated experimentally, and were also calculated with fair to poor agreement with experimental data. By using the experimentally determined stability derivatives, transfer functions were calculated that agreed reasonably well with those calculated by Fourier transformation.

High-Speed Flight Station,
National Advisory Committee for Aeronautics,
Edwards, Calif., May 18, 1955.

REFERENCES

1. Sisk, Thomas R., and Muhleman, Duane O.: Longitudinal Stability Characteristics in Maneuvering Flight of the Convair XF-92A Delta-Wing Airplane Including the Effects of Wing Fences. NACA RM H54J27, 1955.

2. Sisk, Thomas R., and Muhleman, Duane O.: Lateral Stability and Control Characteristics of the Convair XF-92A Delta-Wing Airplane as Measured in Flight. NACA RM H55A17, 1955.

3. Holleman, Euclid C., and Triplett, William C.: Flight Measurements of the Dynamic Longitudinal Stability and Frequency-Response Characteristics of the XF-92A Delta-Wing Airplane. NACA RM H54J26a, 1955.

4. Liddell, Charles J., Jr., Creer, Brent Y., and Van Dyke, Rudolph D., Jr.: A Flight Study of Requirements for Satisfactory Lateral Oscillatory Characteristics of Fighter Aircraft. NACA RM A51E16, 1951.

5. Rosamond, D. L.: Practical Methods for Lateral Stability Analyses. Rep. 2126, McDonnell Aircraft Corp., June 12, 1951.

6. Donegan, James J., Robinson, Samuel W., Jr., and Gates, Ordway B., Jr.: Determination of Lateral-Stability Derivatives and Transfer-Function Coefficients from Frequency-Response Data for Lateral Motions. NACA TN 3083, 1954.

7. Schumacher, Lloyd E.: Methods for Analyzing Transient Flight Data to Obtain Aircraft Frequency Response. (FTD Project No. 49 R1108). Memo. Rep. No. MCRFT-2268, Air Materiel Command, Flight Test Div., Air Force, Jan. 17, 1950.

8. Fisher, Lewis R.: Approximate Corrections for the Effects of Compressibility on the Subsonic Stability Derivatives of Swept Wings. NACA TN 1854, 1949.

9. DeYoung, John, and Harper, Charles W.: Theoretical Symmetric Span Loading at Subsonic Speeds for Wings Having Arbitrary Plan Form. NACA Rep. 921, 1948.

10. Letko, William, and Riley, Donald R.: Effect of an Unswept Wing on the Contribution of Unswept-Tail Configurations to the Low-Speed Static- and Rolling-Stability Derivatives of a Midwing Airplane Model. NACA TN 2175, 1950.

11. DeYoung, John: Theoretical Antisymmetric Span Loading for Wings of Arbitrary Plan Form at Subsonic Speeds. NACA Rep. 1056, 1951. (Supersedes NACA TN 2140.)

12. Toll, Thomas A., and Queijo, M. J.: Approximate Relations and Charts for Low-Speed Stability Derivatives of Swept Wings. NACA TN 1581, 1948.

13. Johnson, Joseph L., Jr.: Low-Speed Measurements of Rolling and Yawing Stability Derivatives of a 60° Delta-Wing Model. NACA RM L54G27, 1954.

14. Cole, Henry A., Jr., Brown, Stuart C., and Holleman, Euclid C.: Experimental and Predicted Longitudinal Response Characteristics of a Large Flexible 35° Swept-Wing Airplane at an Altitude of 35,000 Feet. NACA RM A54H09, 1954.

TABLE I

PHYSICAL CHARACTERISTICS OF THE XF-92A AIRPLANE

Wing:	
Area, sq ft	425
Span, ft	31.33
Airfoil section	NACA $65_{(06)}$-006.5
Mean aerodynamic chord, ft	18.09
Aspect ratio	2.31
Root chord, ft	27.13
Tip chord	0
Taper ratio	0
Sweepback (leading edge), deg	60
Incidence, deg	0
Dihedral (chord plane), deg	0
Elevons:	
Area (total, both, aft of hinge line), sq ft	76.19
Span (one elevon), ft	13.35
Chord (aft of hinge line, constant except at tip), ft	3.05
Movement, deg	
Elevator:	
Up	15
Down	5
Aileron, total	10
Operation	Hydraulic
Vertical tail:	
Area, sq ft	75.35
Height, above fuselage center line, ft	11.50
Rudder:	
Area, sq ft	15.53
Span, ft	9.22
Travel, deg	±8.5
Operation	Hydraulic
Fuselage:	
Length, ft	42.80
Power plant:	
Engine	Allison J33-A-29 with afterburner
Rating:	
Static thrust at sea level, lb	5,600
Static thrust at sea level with afterburner, lb	7,500
Weight:	
Gross weight (560 gal fuel), lb	15,560
Empty weight, lb	11,808
Center-of-gravity locations:	
Gross weight (560 gal fuel), percent M.A.C.	25.5
Empty weight, percent M.A.C.	29.2

TABLE II

EFFECT OF VARYING CERTAIN CALCULATED DERIVATIVES ON THE

EXPERIMENTALLY DETERMINED DERIVATIVES

Calculated derivatives			Experimental derivatives			
C_{Y_β}	C_{n_p}	C_{l_r}	C_{l_β}	C_{l_p}	C_{n_r}	C_{n_β}
-0.70	-0.001	0.071	-0.0648	-0.144	-0.309	0.330
-.70	-.001	.085	-.0648	-.142	-.308	.329
-.70	-.0012	.071	-.0648	-.144	-.321	.327
-.84	-.001	.071	-.0622	-.137	-.294	.329

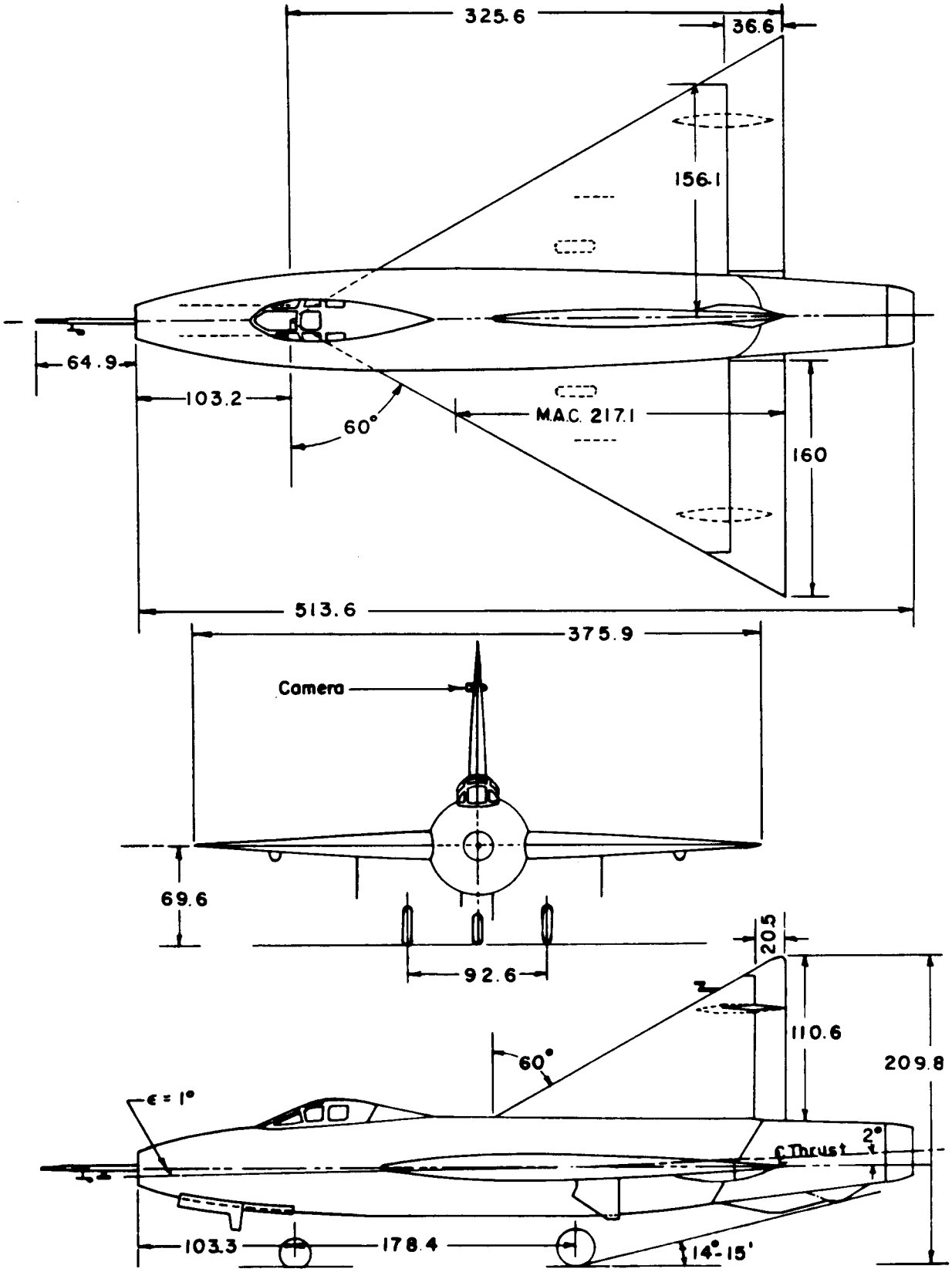

Figure 1.- Three-view drawing of the XF-92A airplane. All dimensions in inches.

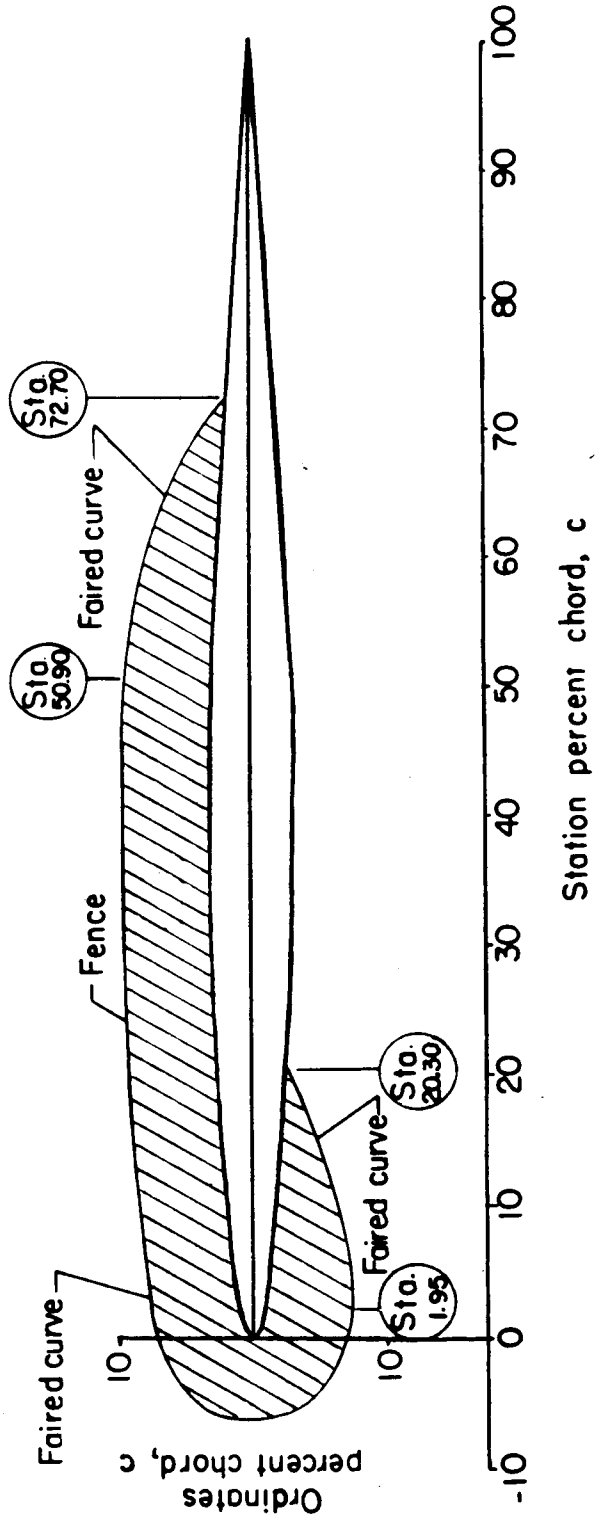

Figure 2.- Details of the wing fences tested. Fence located at 0.607 wing semispan (114.10 in.); wing chord at fence station = 127.94 inches; maximum wing thickness at fence station = 8.32 inches.

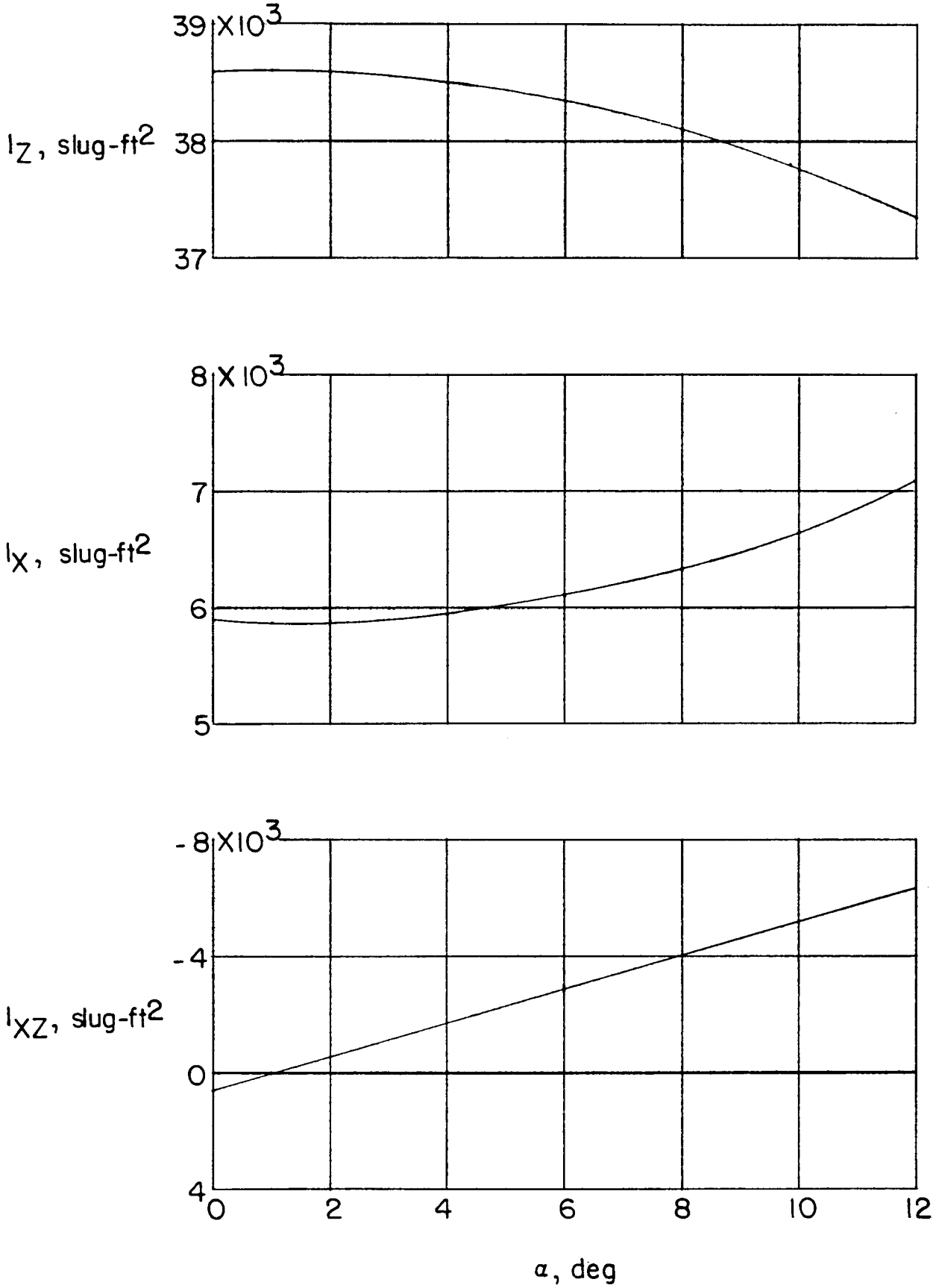

Figure 3.- Assumed variation of airplane inertia with angle of attack.

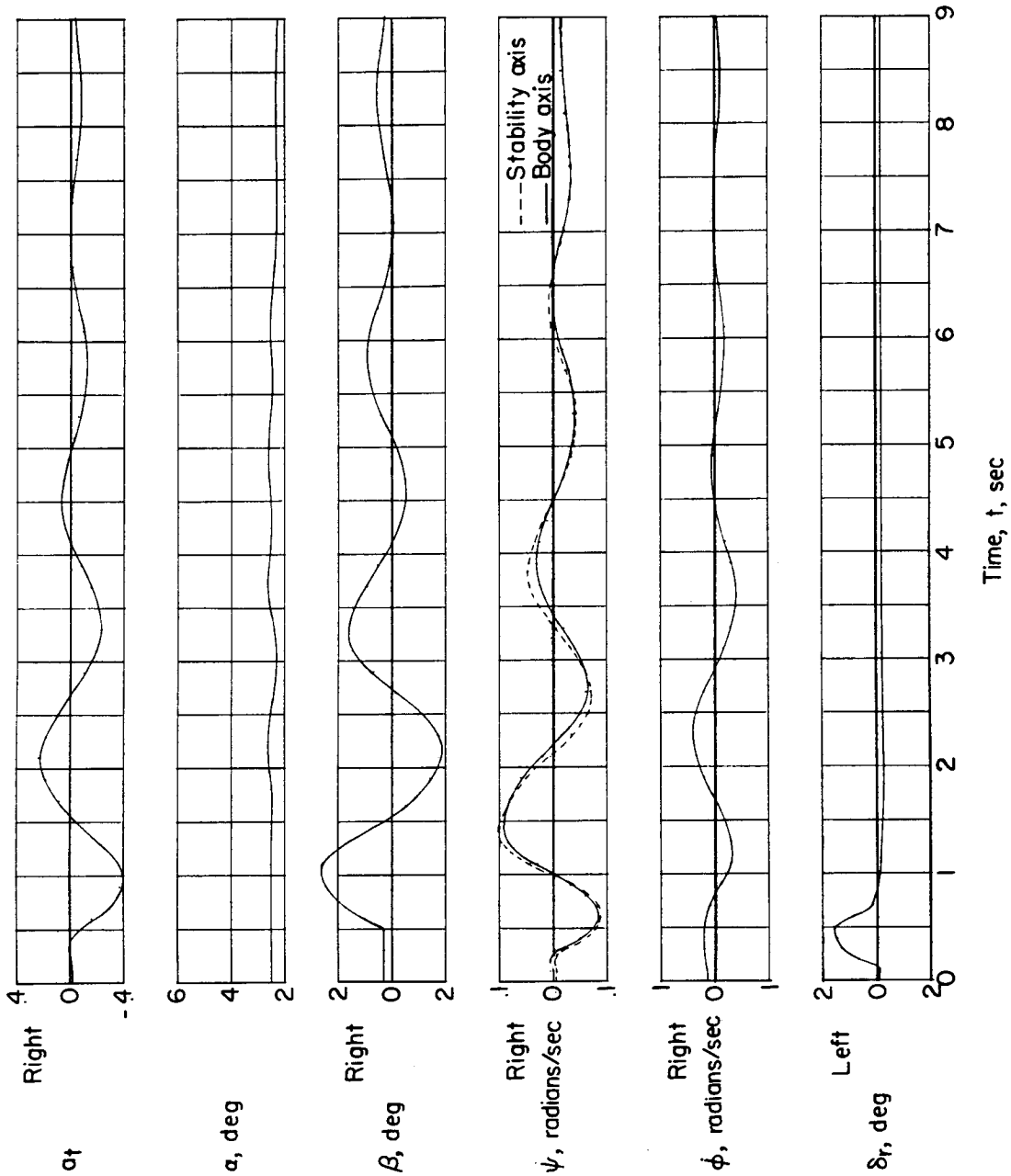

(a) M = 0.87; $h_p \approx 30,000$ feet.

Figure 4.- Typical time history of the test maneuver.

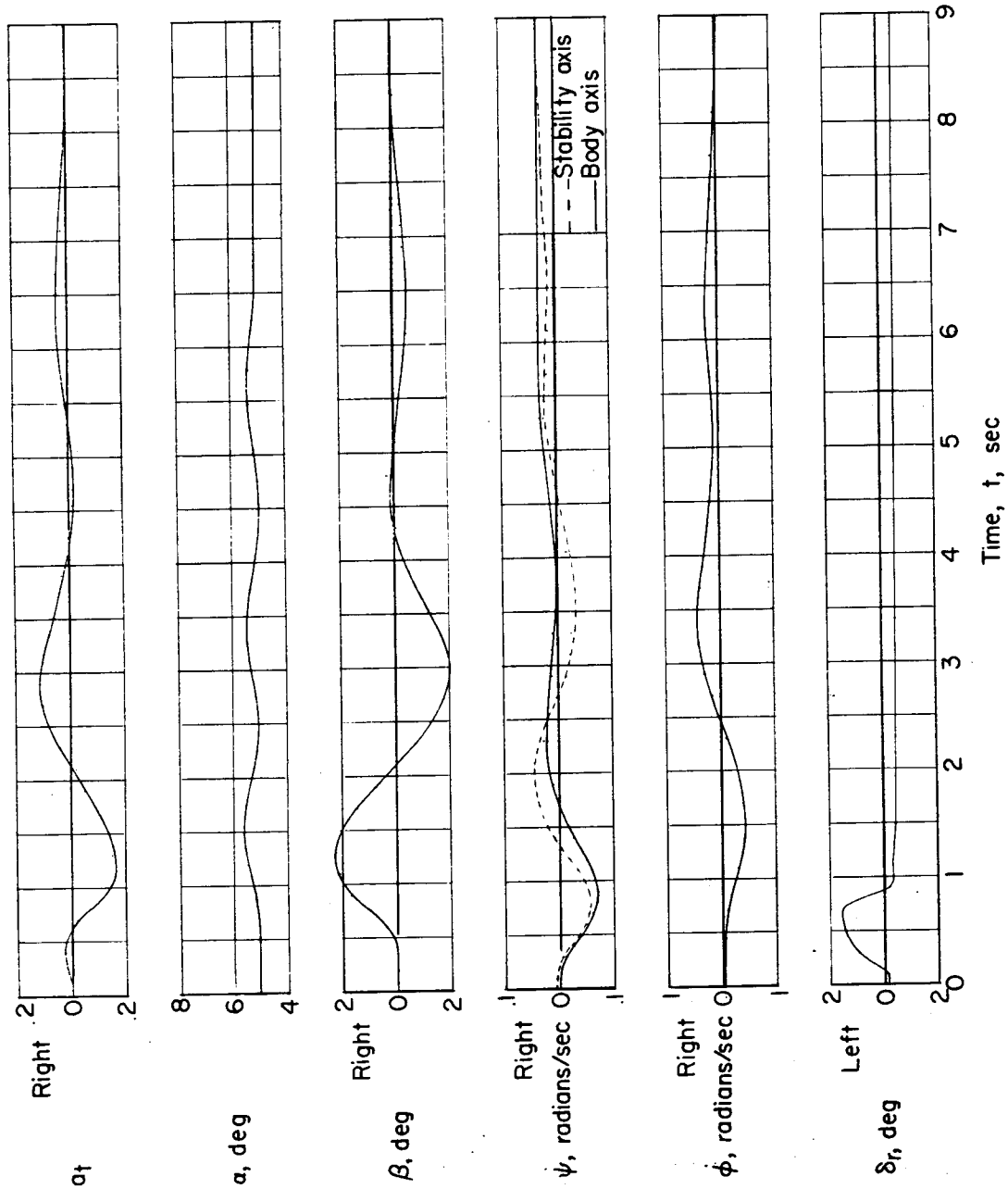

(b) M = 0.52; $h_p \approx 30,000$ feet.

Figure 4.- Concluded.

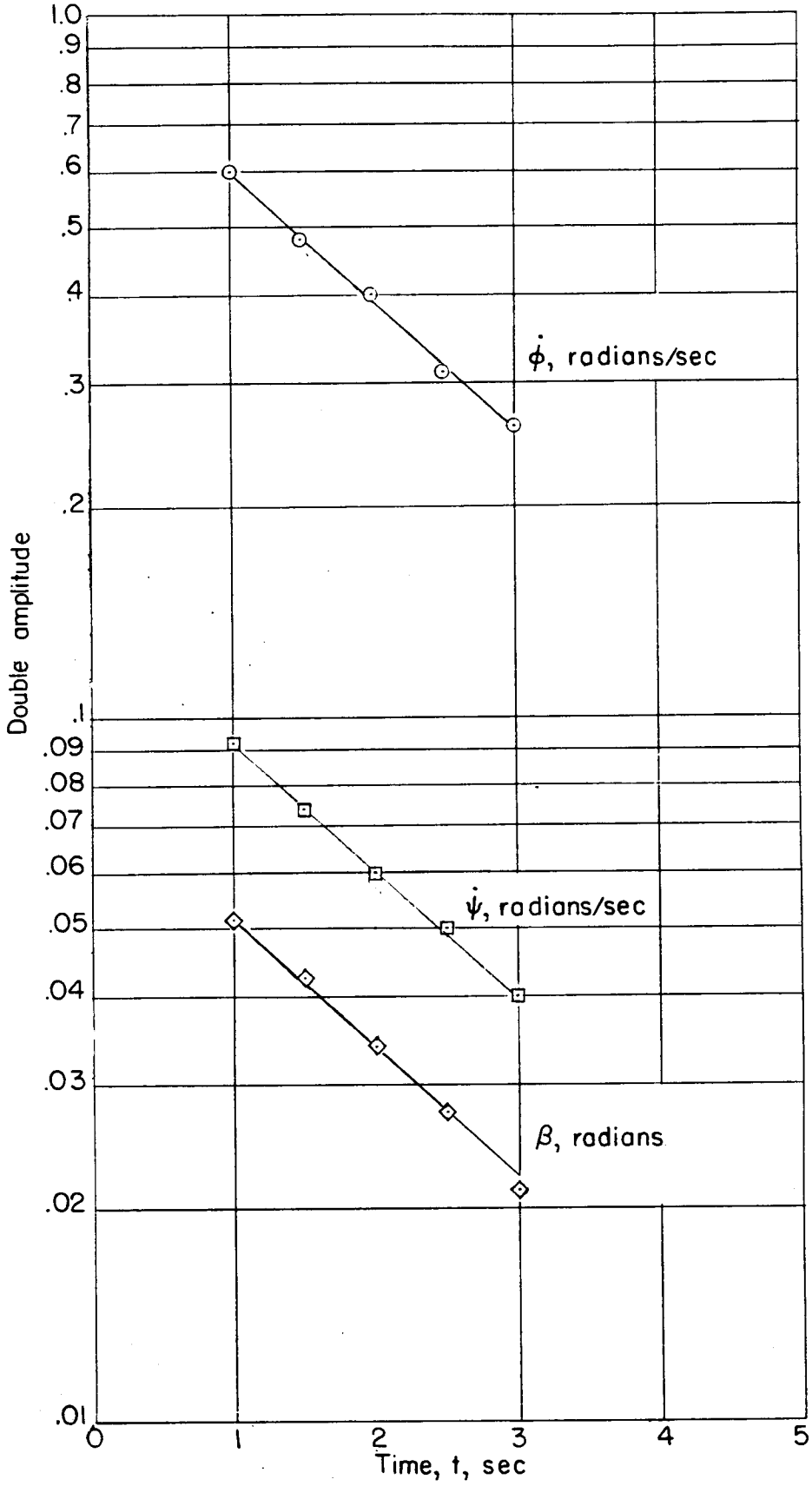

Figure 5.- Verification of the logarithmic order of the airplane oscillation.

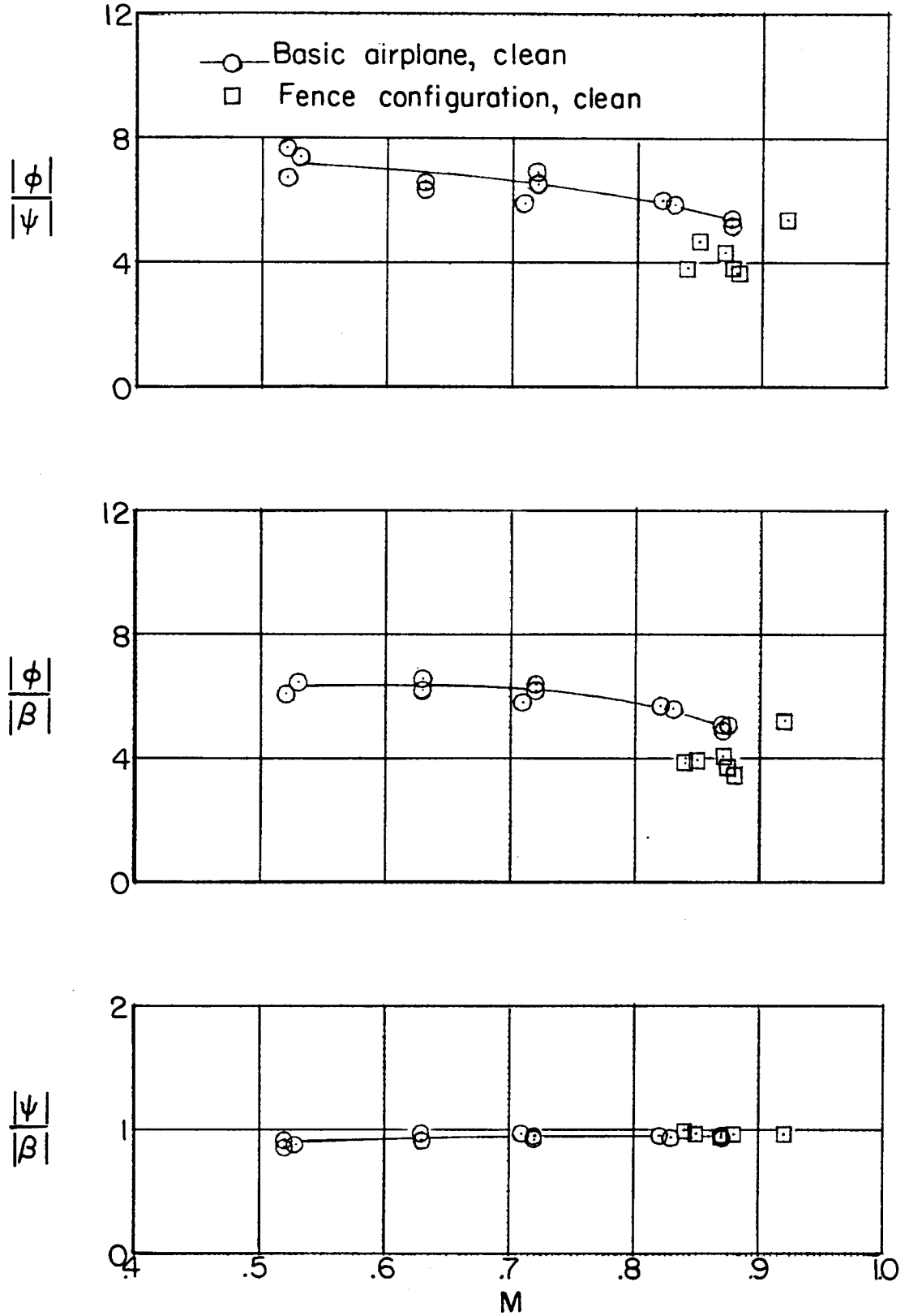

Figure 6.- Amplitude ratio at the natural frequency of roll to yaw, roll to sideslip, and yaw to sideslip for the airplane at an altitude of 30,000 feet (stability axis).

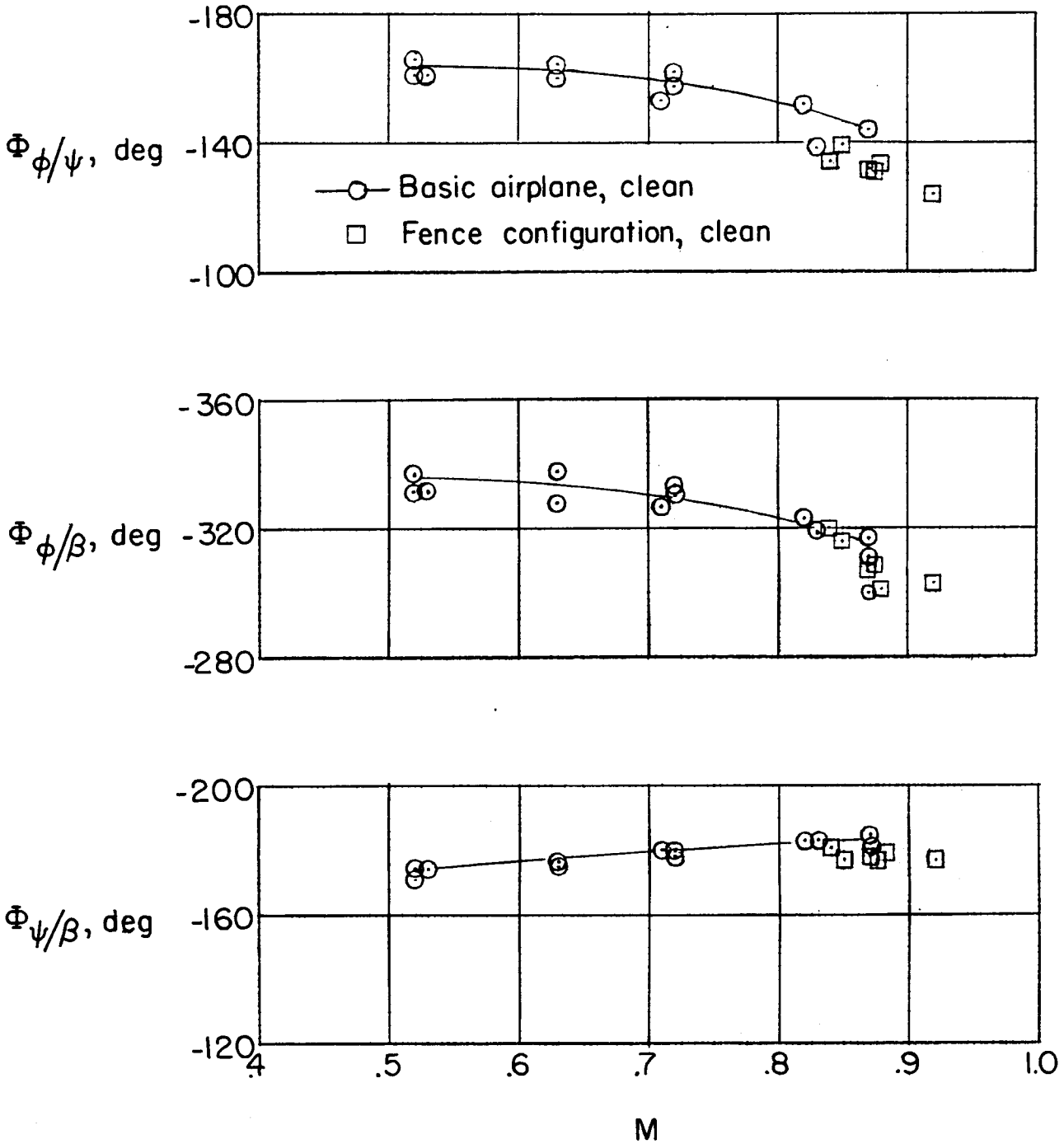

Figure 7.- Phase angle relationships at the natural frequency of roll, yaw, and sideslip at an altitude of 30,000 feet (stability axis).

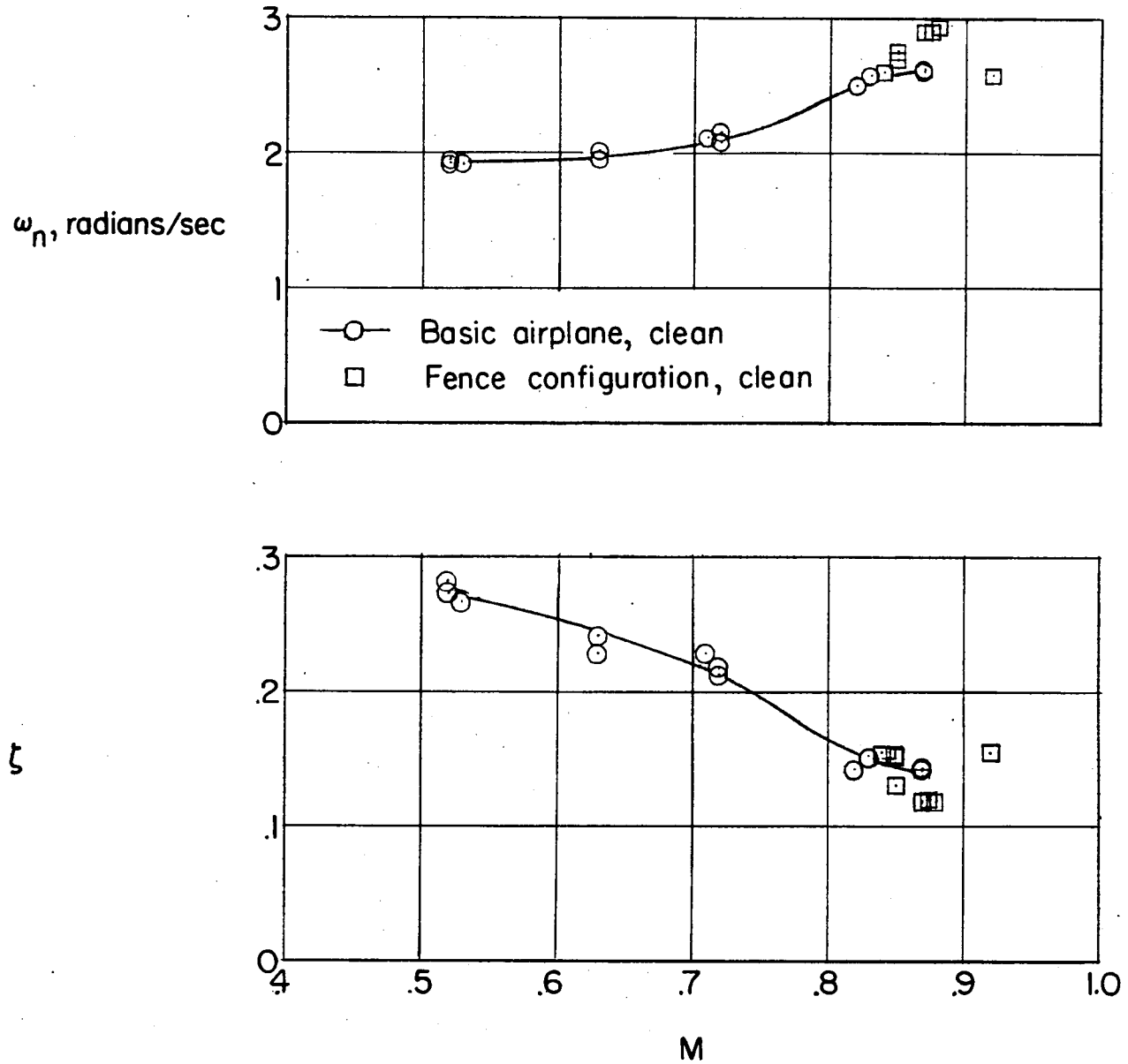

Figure 8.- Undamped natural frequency and damping ratio at an altitude of 30,000 feet.

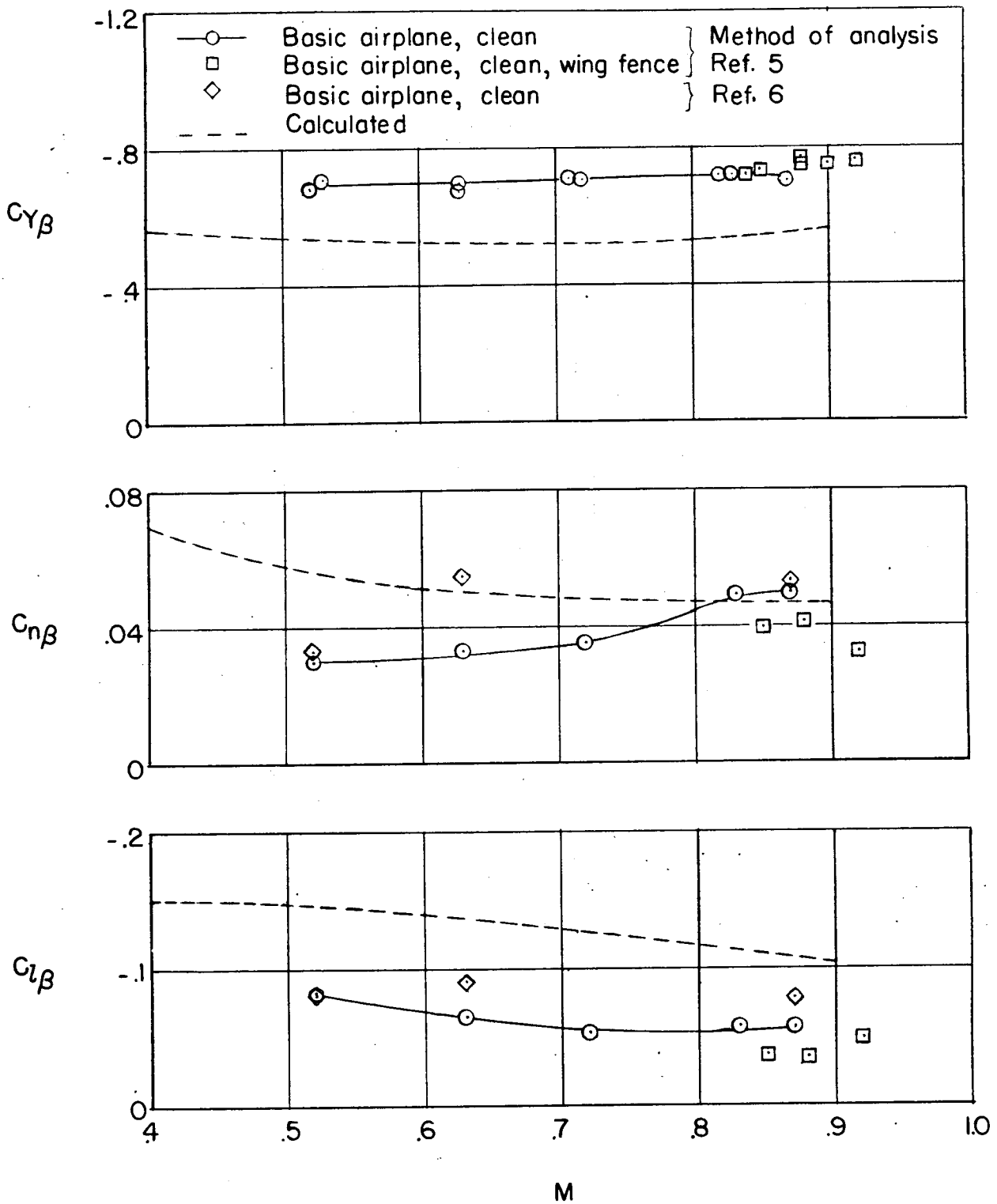

(a) Sideslip derivatives.

Figure 9.- Experimental and calculated stability derivatives for the XF-92A airplane.

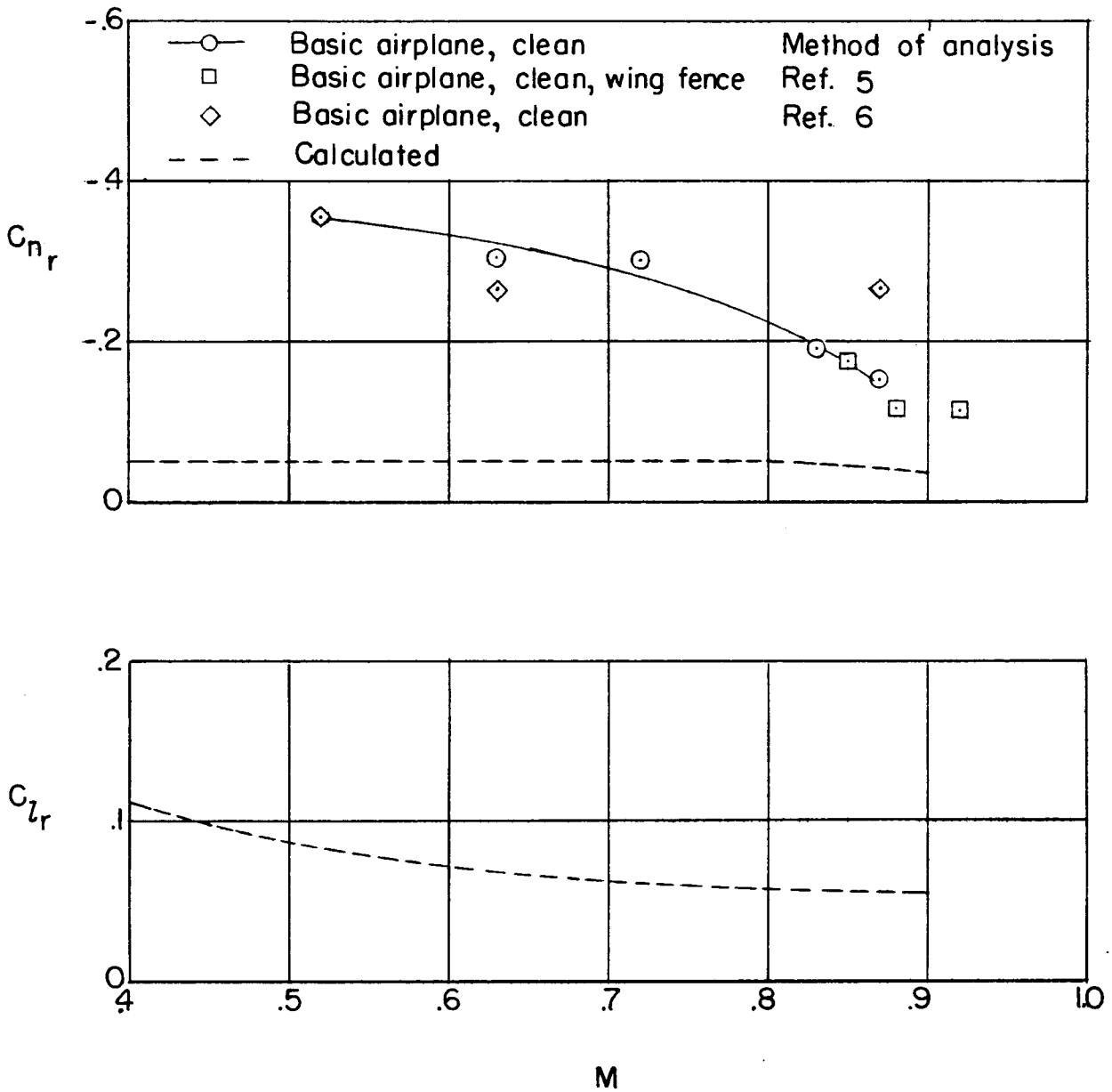

(b) Yawing derivatives.

Figure 9.- Continued.

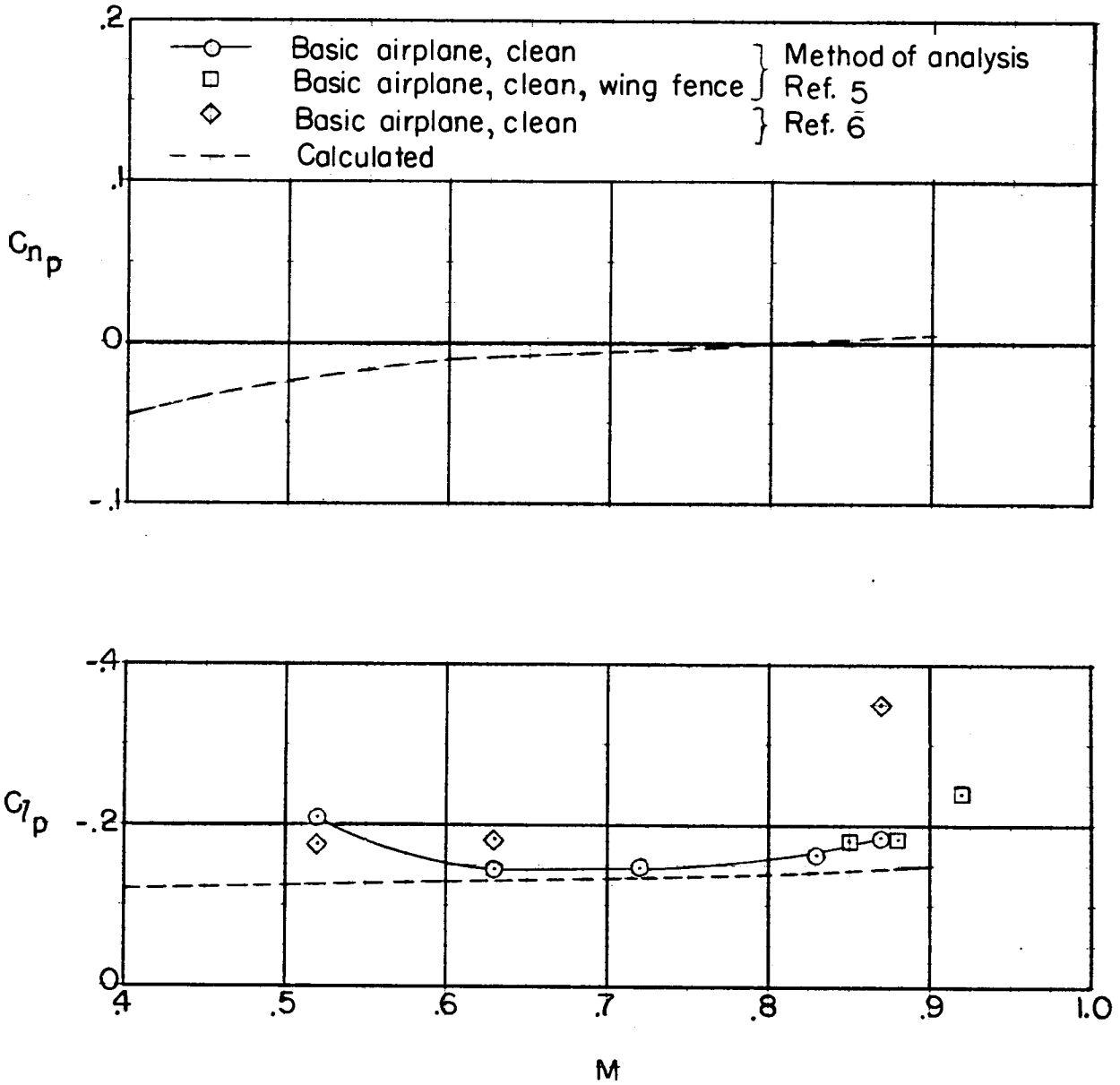

(c) Rolling derivatives.

Figure 9.- Concluded.

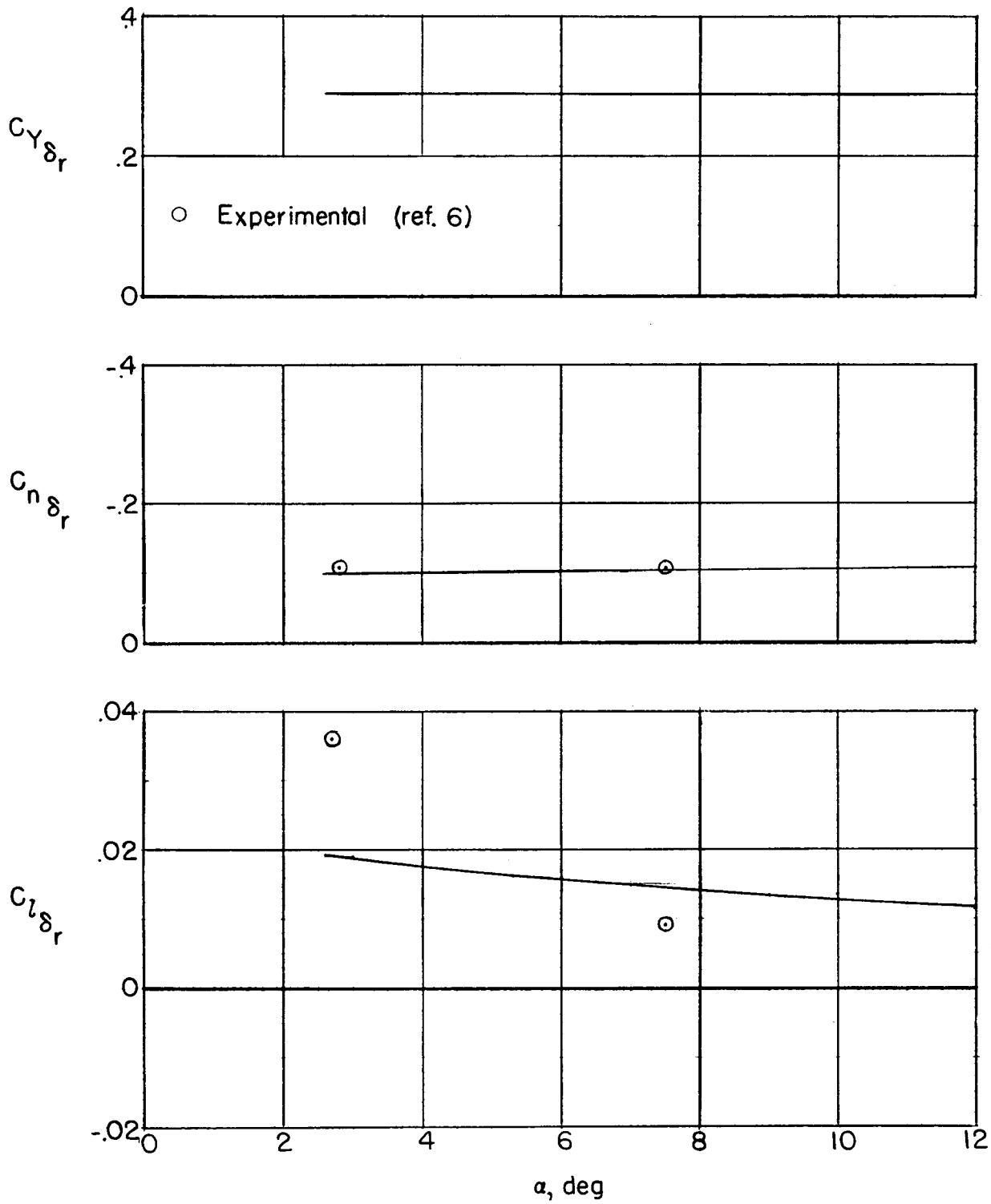

Figure 10.- Control effectiveness from the Ames 40- by 80-foot wind-tunnel tests.

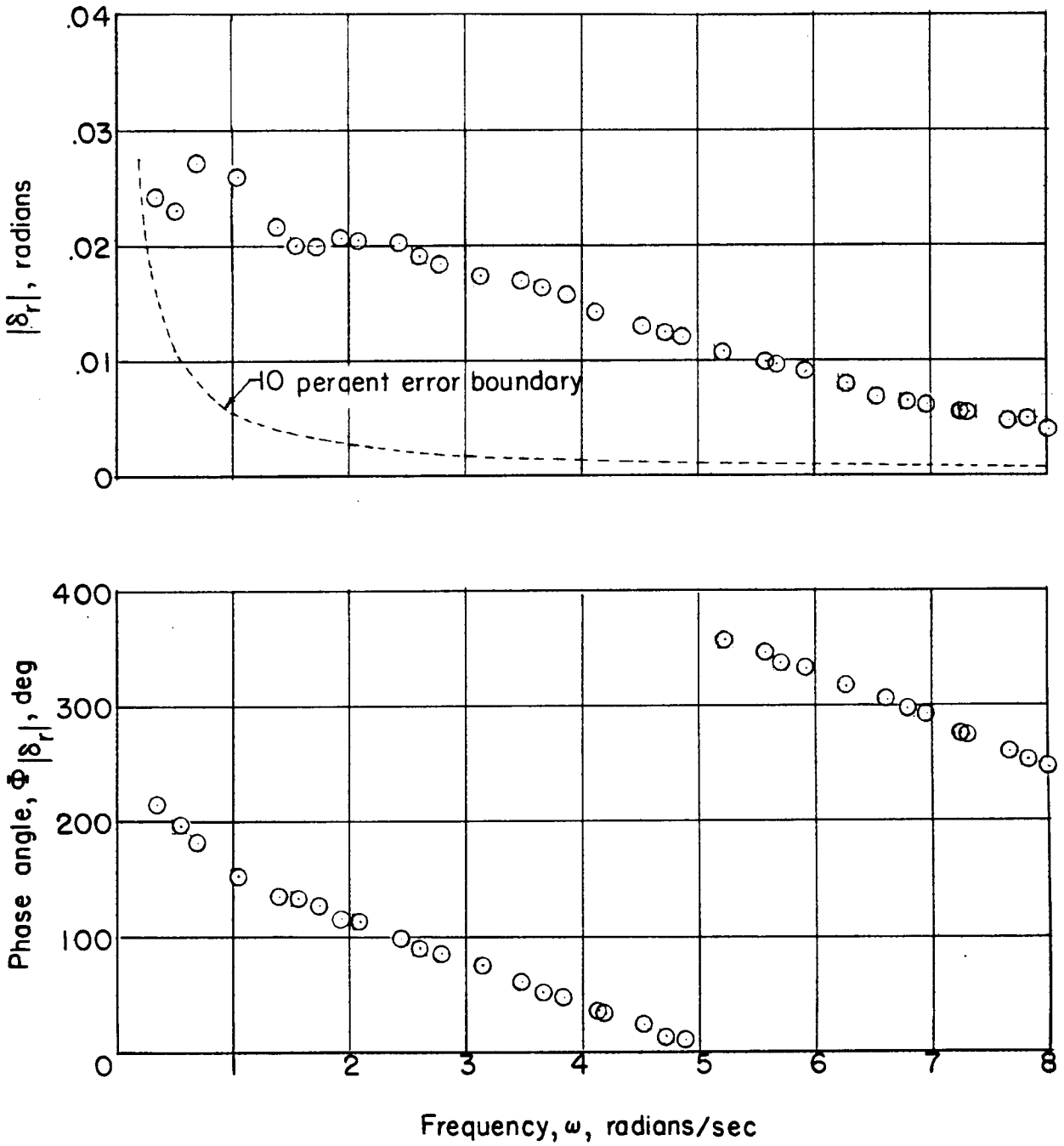

(a) Rudder position.

Figure 11.- The frequency content of a typical run.

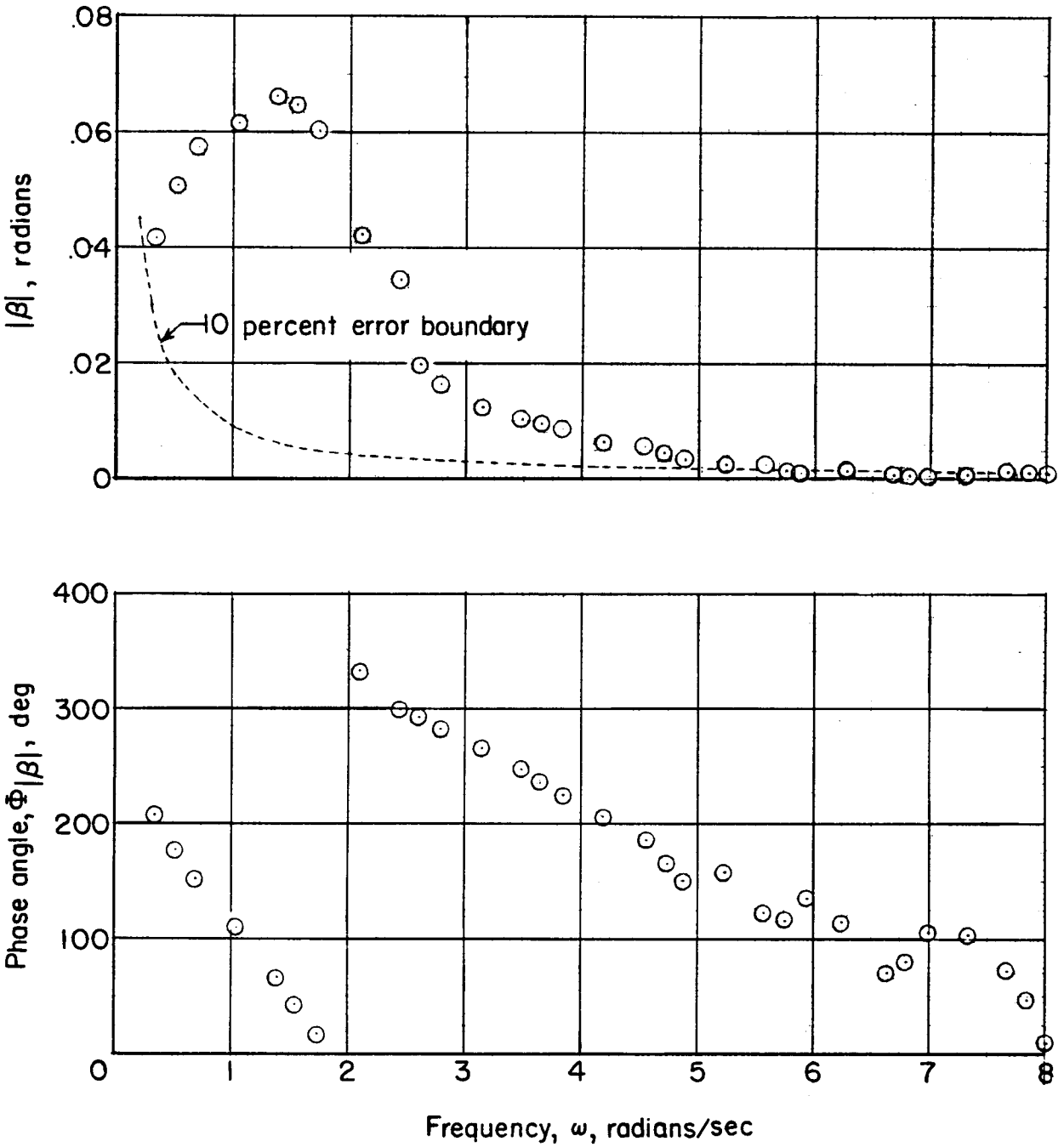

(b) Sideslip angle.

Figure 11.- Continued.

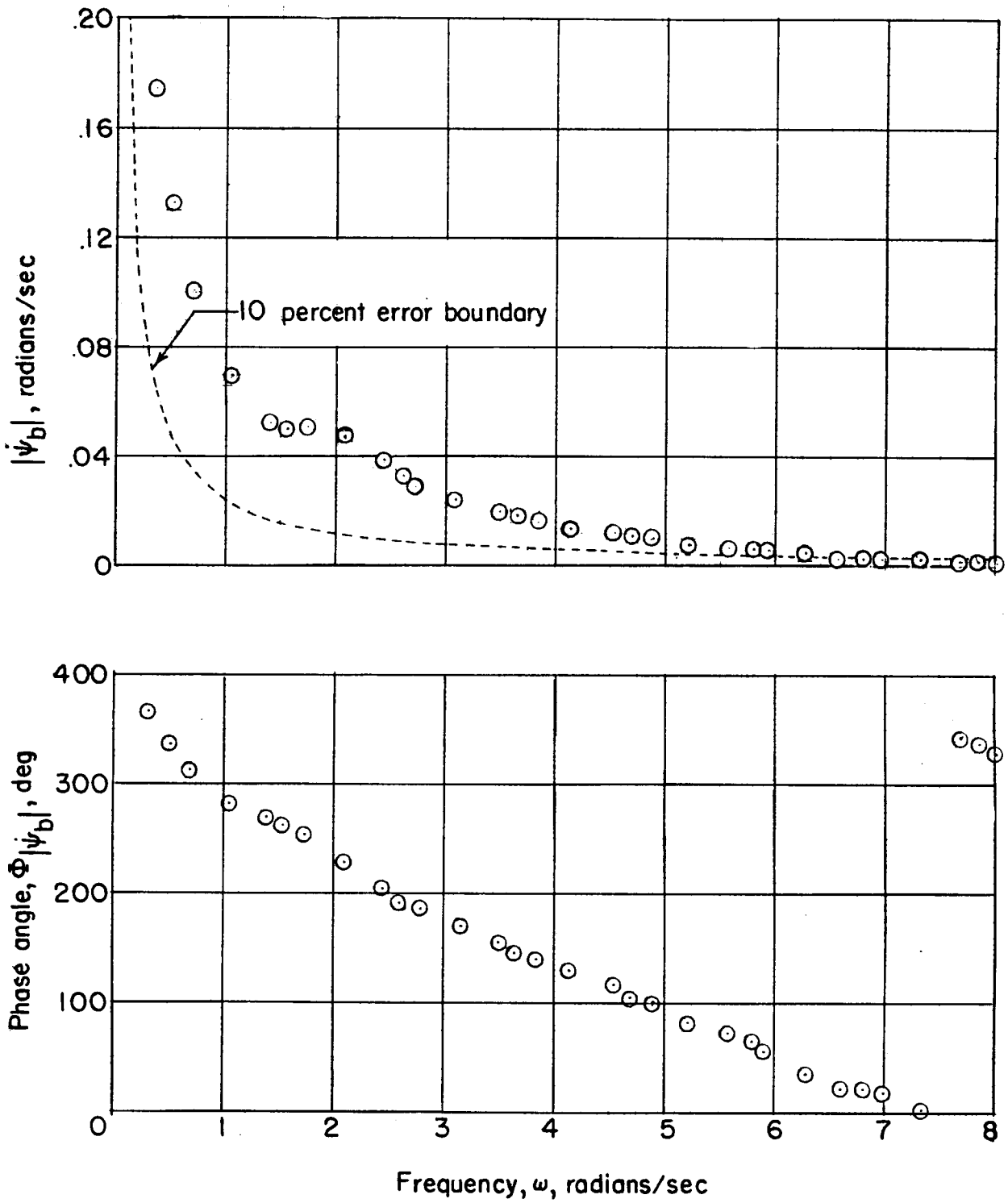

(c) Yawing velocity.

Figure 11.- Continued.

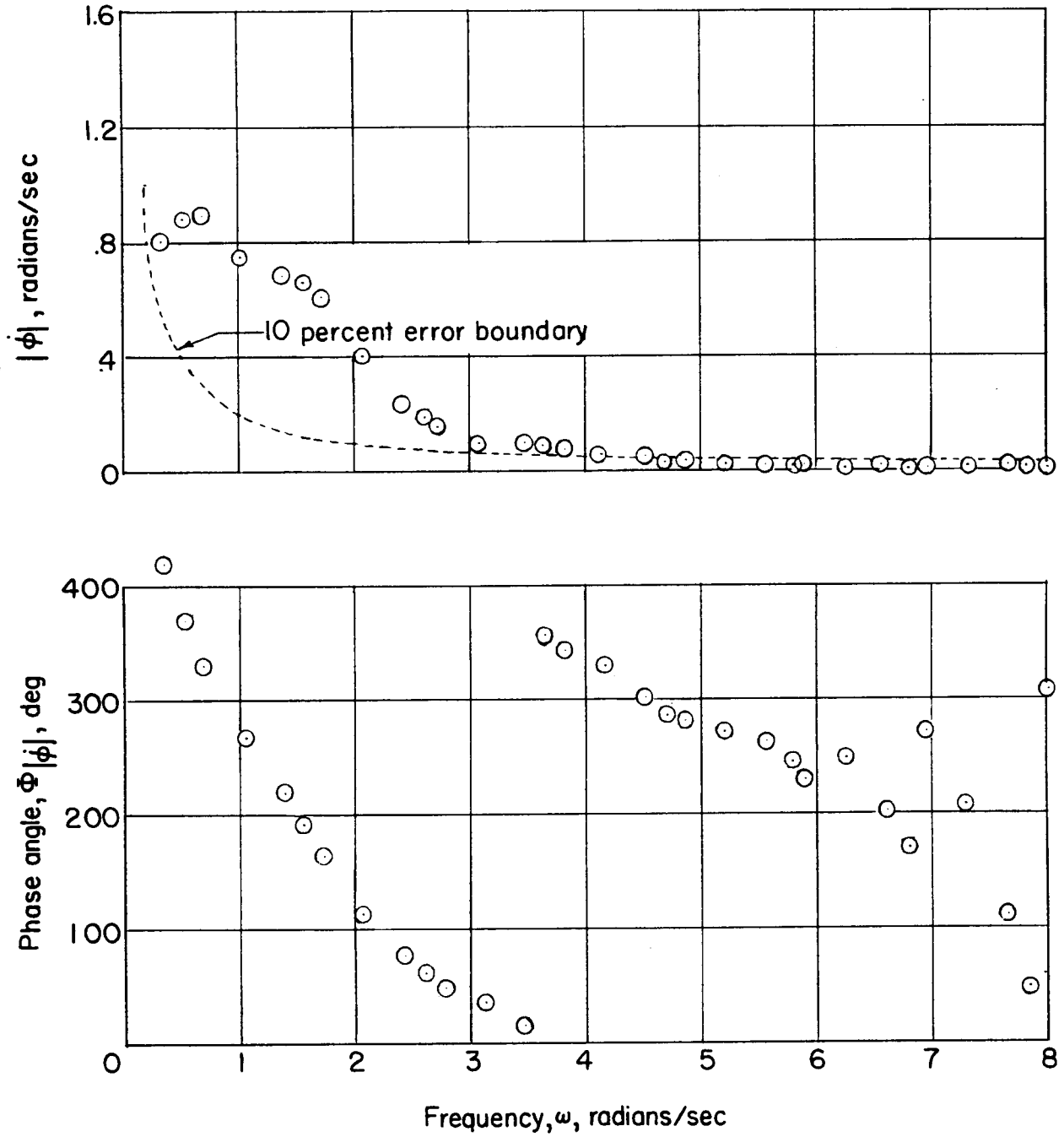

(d) Rolling velocity.

Figure 11.- Concluded.

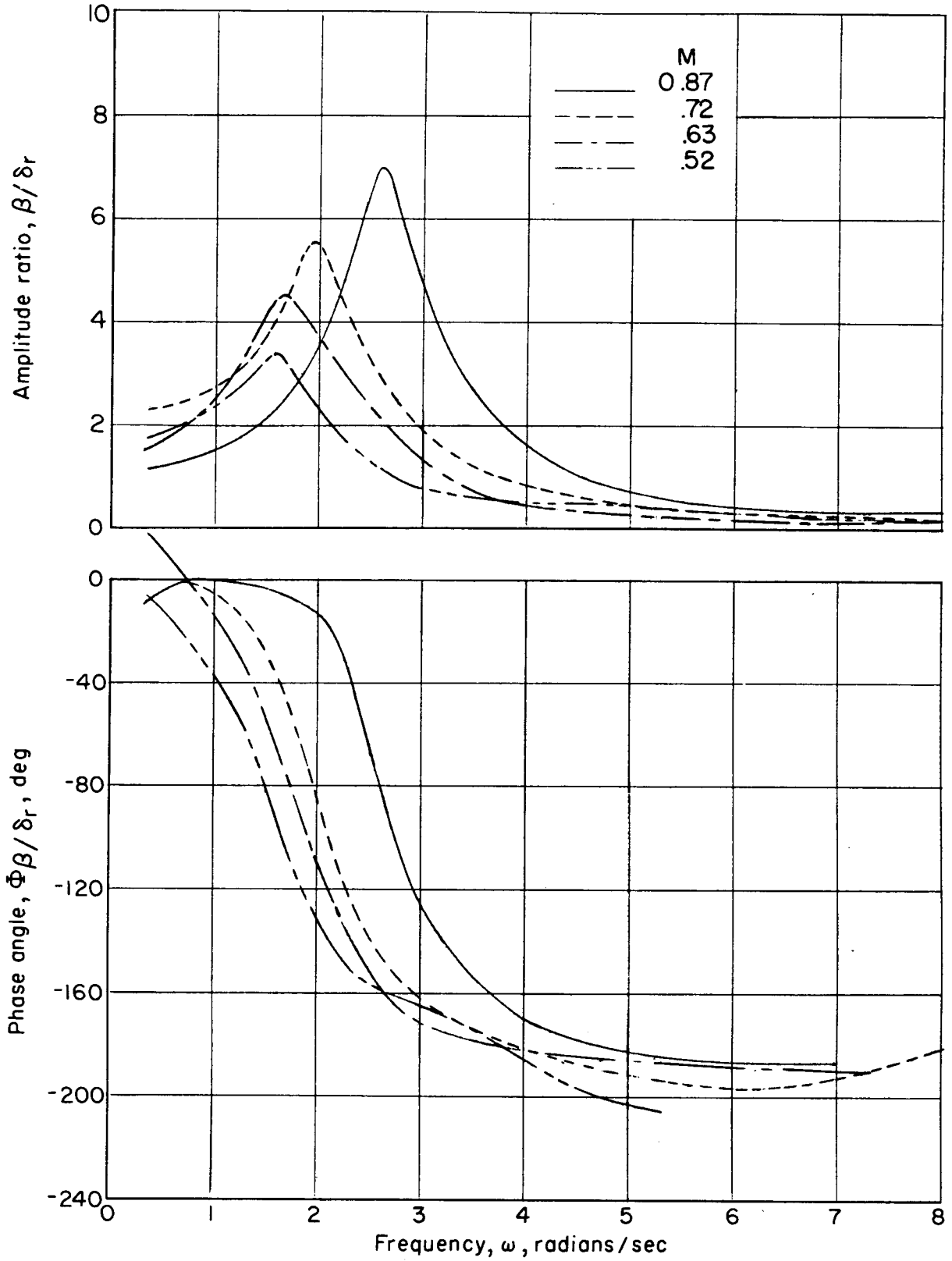

(a) Sideslip angle.

Figure 12.- Frequency response characteristics of the XF-92A airplane at an altitude of 30,000 feet.

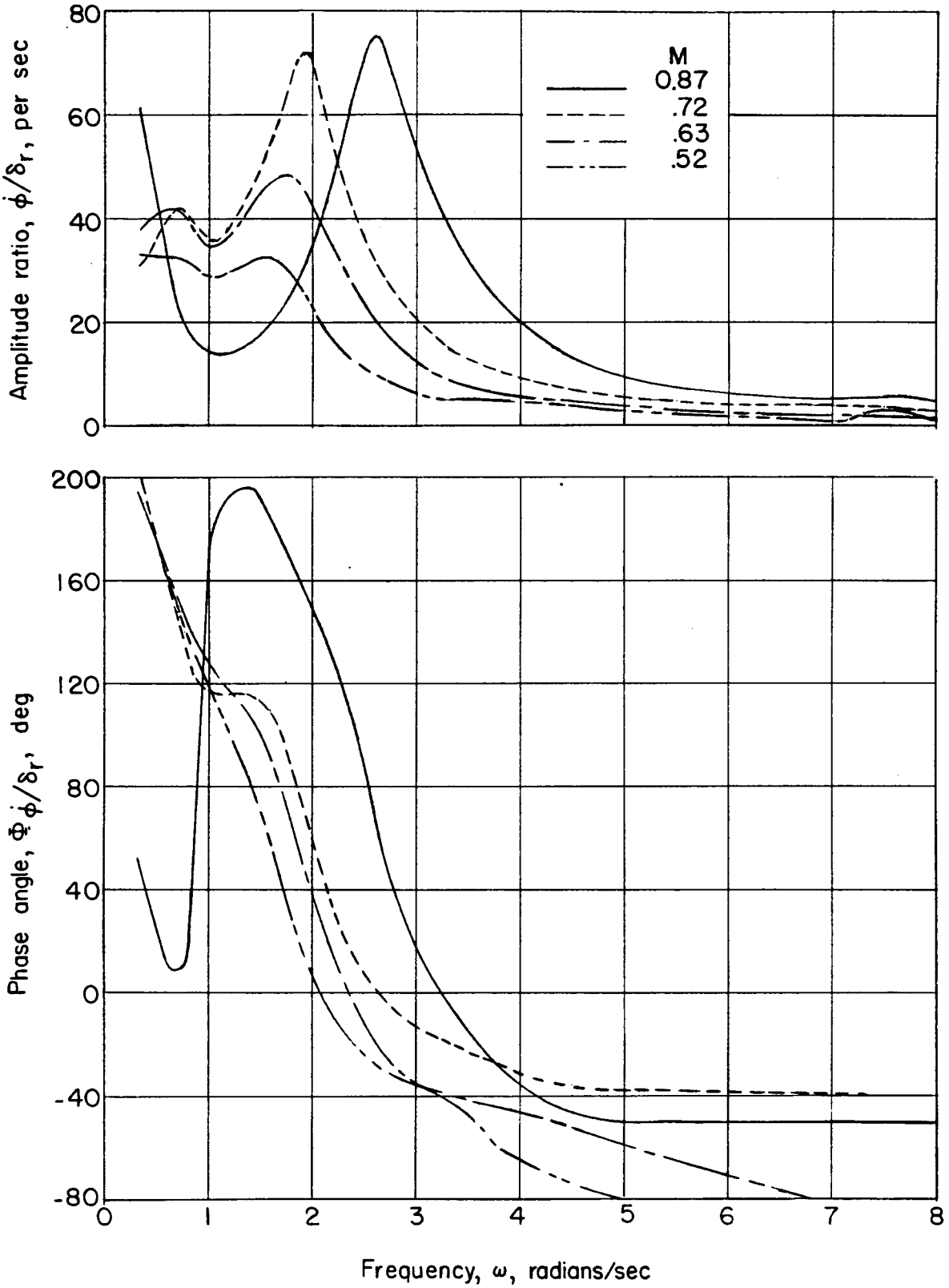

(b) Rolling velocity.

Figure 12.- Continued.

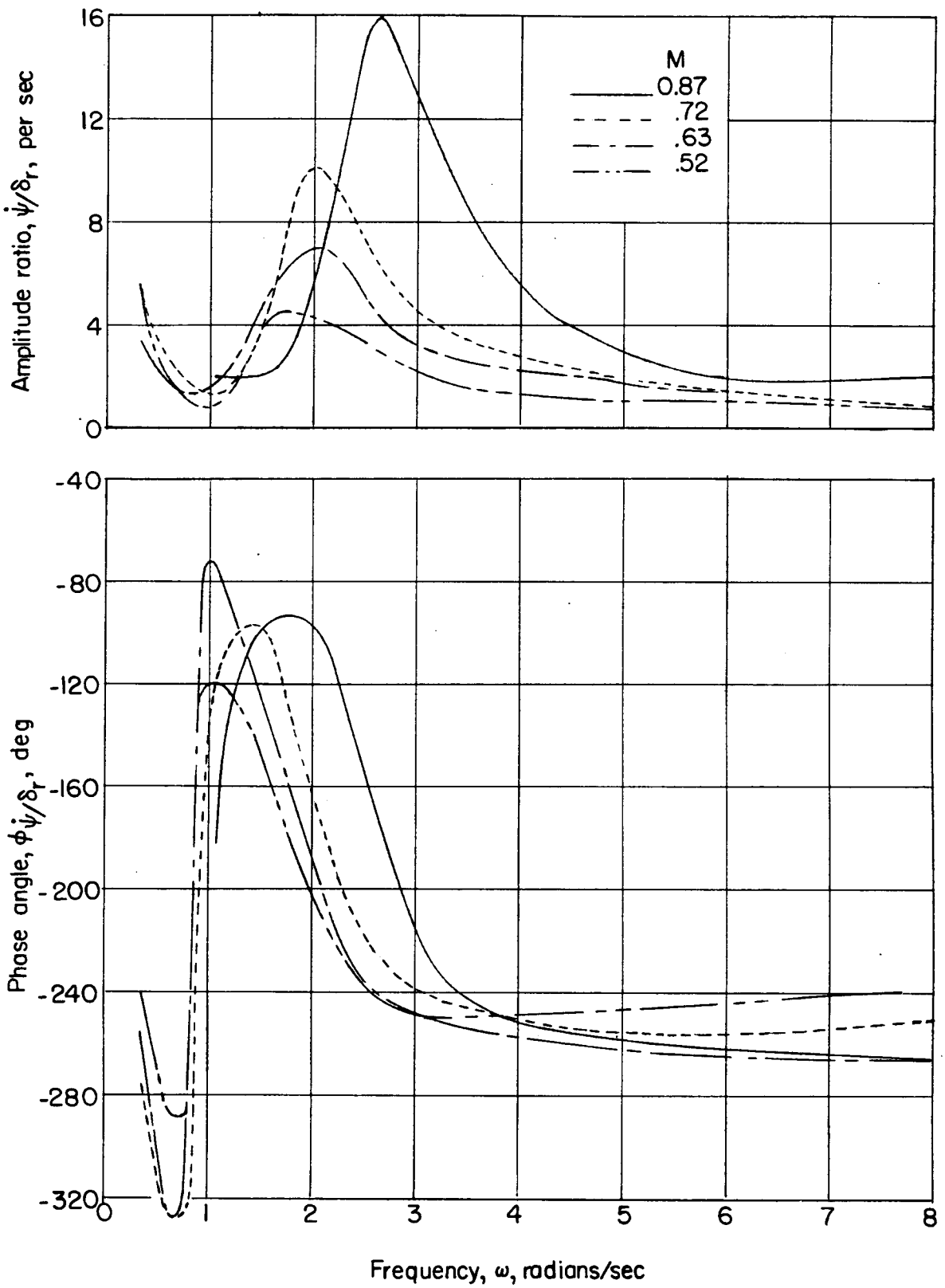

(c) Yawing velocity.

Figure 12.- Continued.

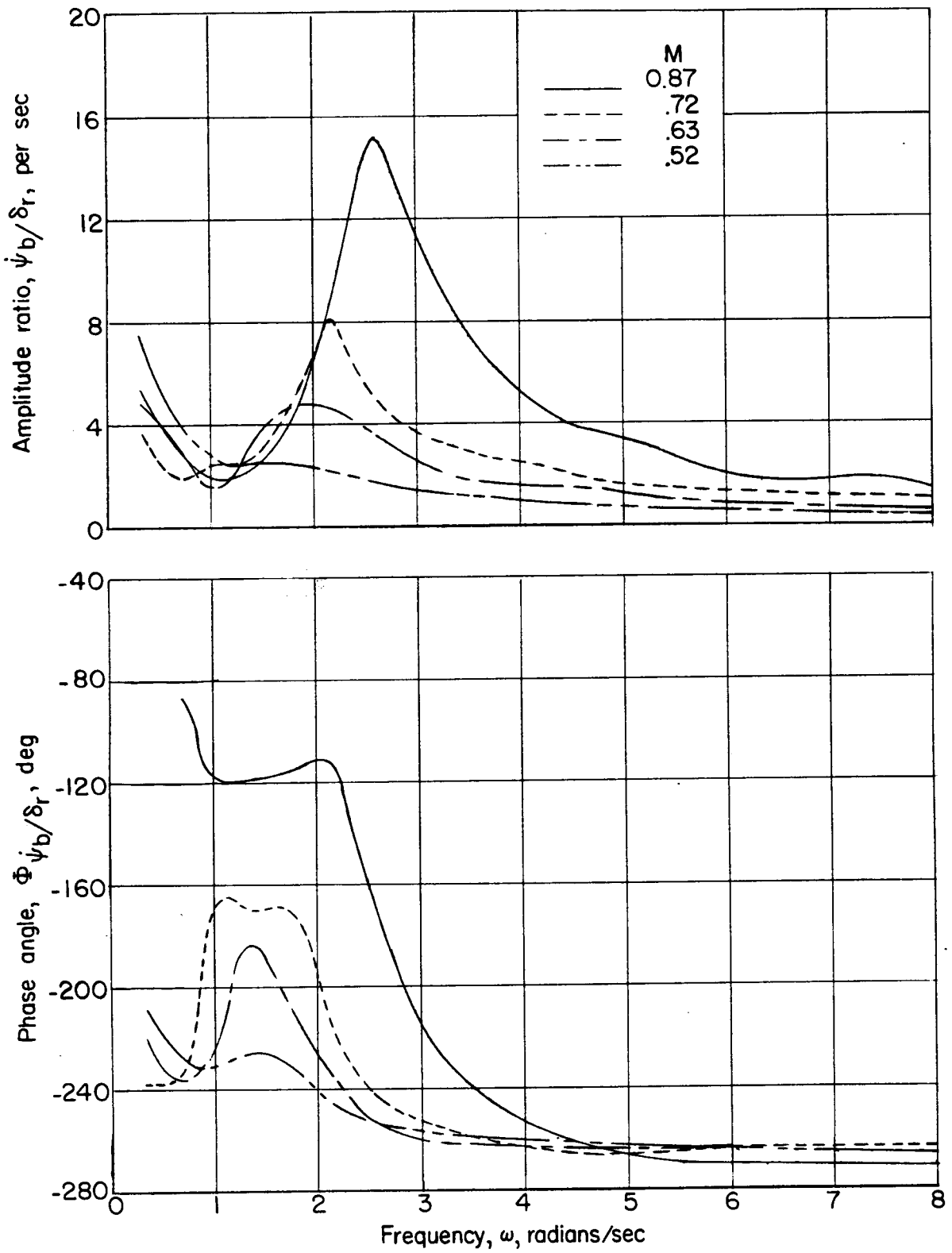

(d) Yawing velocity about the airplane body axis.

Figure 12.- Concluded.

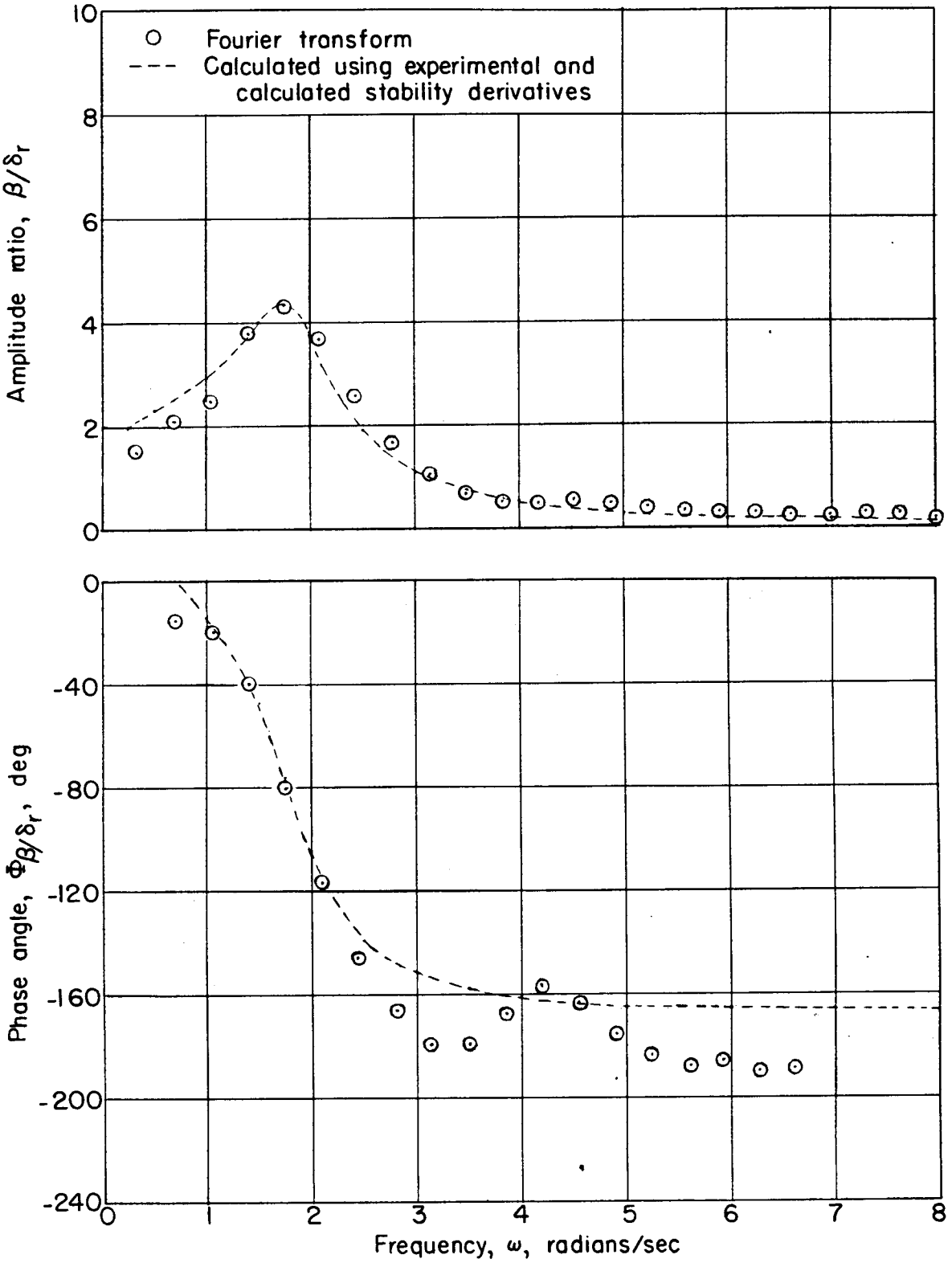

(a) Sideslip angle.

Figure 13.- Comparison of the airplane frequency response calculated by Fourier transformation and from airplane stability derivatives.

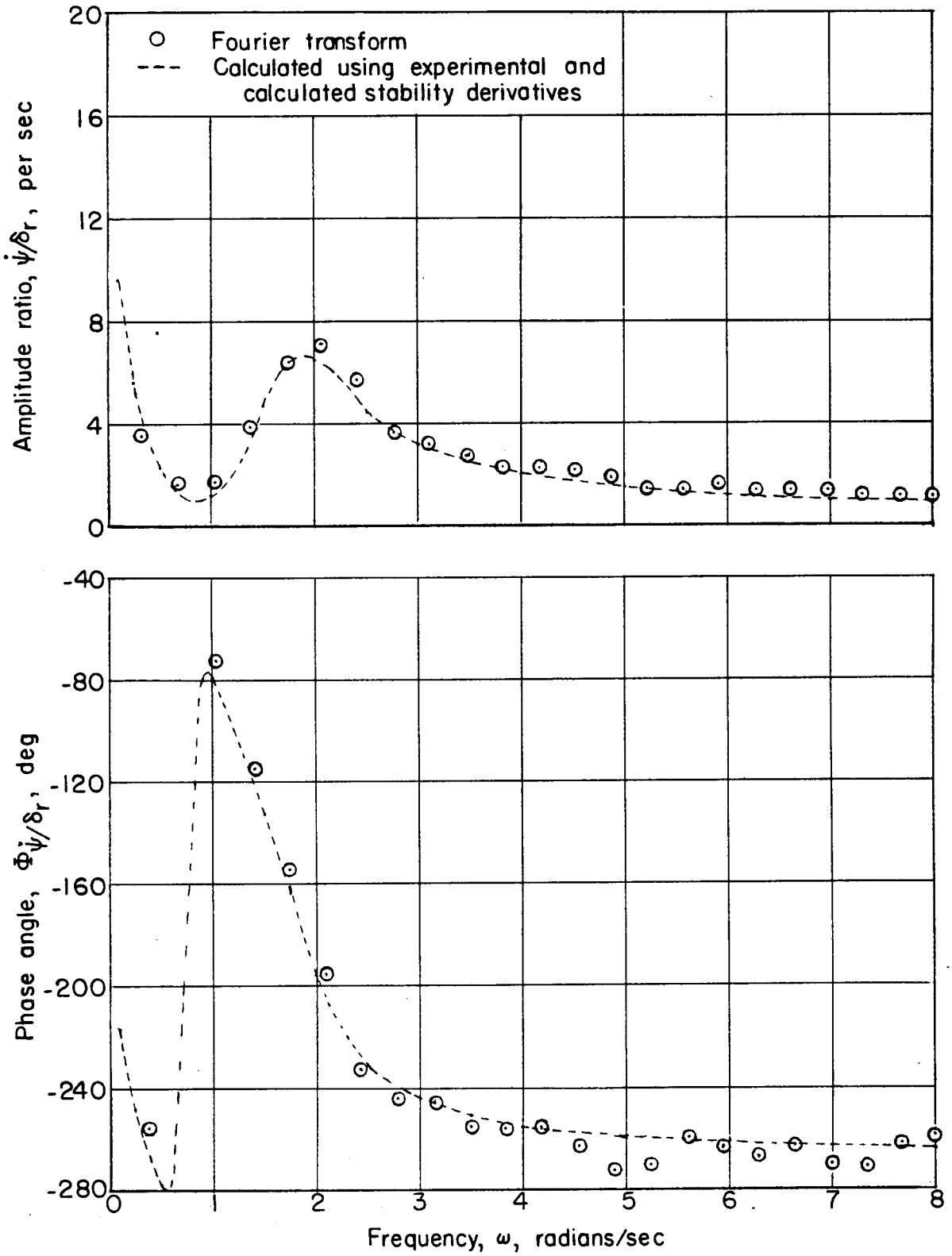

(b) Yawing velocity.

Figure 13.- Continued.

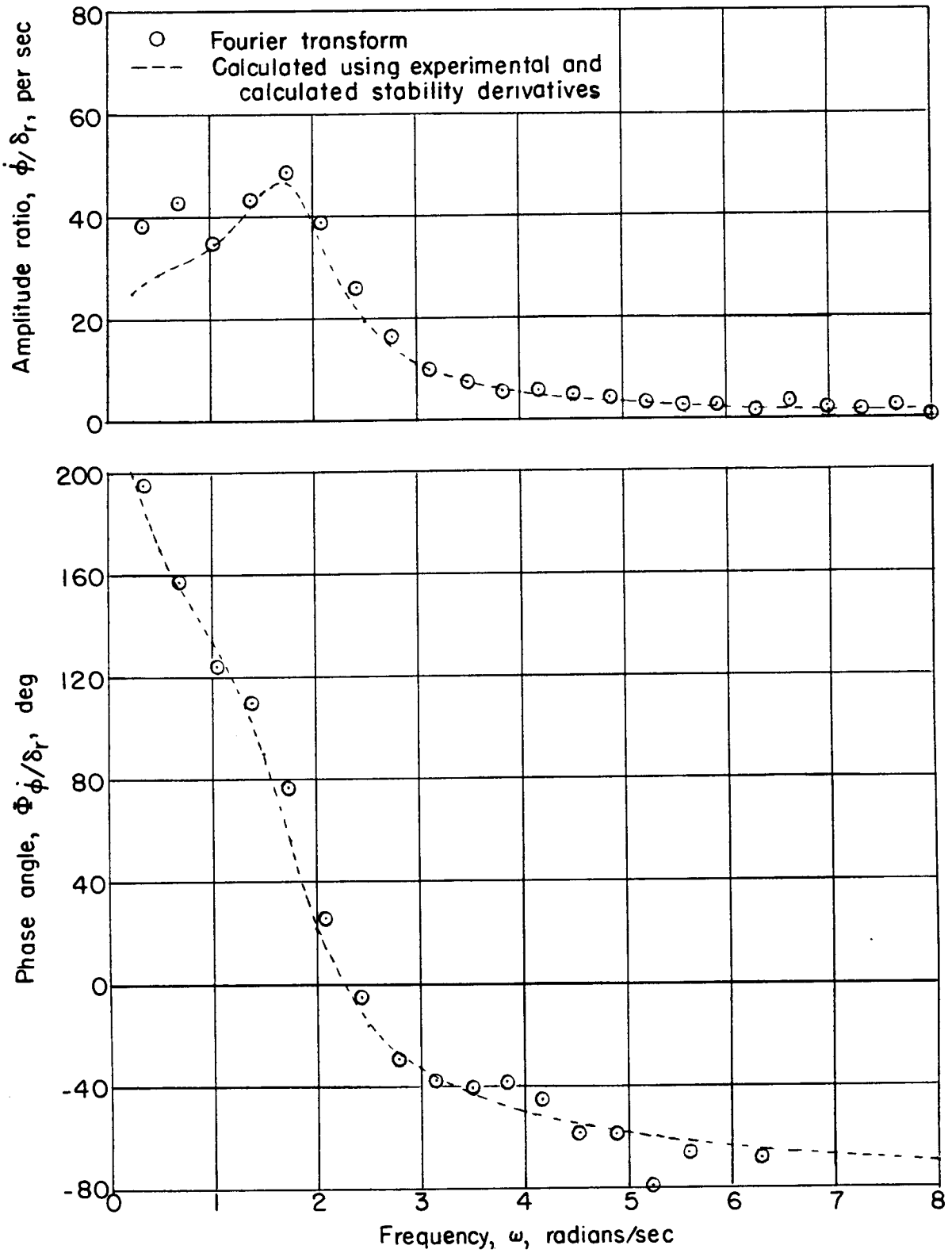

(c) Rolling velocity.

Figure 13.- Concluded.

NACA - Langley Field, Va.